

## Article

# Output Feedback Control of Sine-Gordon Chain over the Limited Capacity Digital Communication Channel

Boris Andrievsky <sup>1,2,\*</sup> , Yury Orlov <sup>1,3</sup>  and Alexander L. Fradkov <sup>1,2</sup> 

- <sup>1</sup> Control of Complex Systems Laboratory, Institute for Problems in Mechanical Engineering of Russian Academy of Sciences (IPME RAS), 61 Bol'shoy Pr. V.O., 199178 Saint Petersburg, Russia; yorlov@cicese.mx (Y.O.); abr@ipme.ru or alf@ipme.ru (A.L.F.)
- <sup>2</sup> Faculty of Mathematics and Mechanics, Saint-Petersburg State University, Stary Peterhof, Universitetsky Prospekt, 198504 Saint Petersburg, Russia
- <sup>3</sup> Department of Electronics and Telecommunications, Mexican Scientific Research and Advanced Studies Center of Ensenada, Ensenada 22860, Mexico
- \* Correspondence: b.andrievsky@spbu.ru; Tel.: +7-812-321-4776

**Abstract:** With the digitalization of mechatronic systems in the conditions of a shortage of available bandwidth of digital communication channels, the problem of ensuring the transfer of information between various components of the system can arise. This problem can be especially challenging in the observation and control of spatially distributed objects due to the complexity of their dynamics, wide frequency band, and other factors. In such cases, a useful approach is to employ smart sensors, in which the measurement results are encoded for transmission over a digital communication channel. Specifically, the article is focused on the transmission of measurement data for the control of energy for a spatially-distributed sine-Gordon chain. The procedures for binary coding of measurements by first- and full-order coder-decoder pairs are proposed and numerically investigated, for each of which the use of stationary and adaptive coding procedures is studied. The procedures for estimating the state of the circuit when measuring outputs are studied, and for each of them, the accuracy of not only estimating the state but also controlling the system by output with the help of an observer is considered. The results of comparative modeling are presented, demonstrating the dependence of the accuracy of estimation and control on the data transfer rate.

**Keywords:** sine-Gordon equation; digitalization; energy control; speed-gradient; quantization; data sampling; communication constraints



**Citation:** Andrievsky, B.; Orlov, Y.; Fradkov, A.L. Output Feedback Control of Sine-Gordon Chain over the Limited Capacity Digital Communication Channel. *Electronics* **2023**, *12*, 2269. <https://doi.org/10.3390/electronics12102269>

Academic Editors: Erik Kučera, Štefan Kozák and Teofana Puleva

Received: 3 April 2023  
Revised: 4 May 2023  
Accepted: 12 May 2023  
Published: 17 May 2023



**Copyright:** © 2023 by the authors. Licensee MDPI, Basel, Switzerland. This article is an open access article distributed under the terms and conditions of the Creative Commons Attribution (CC BY) license (<https://creativecommons.org/licenses/by/4.0/>).

## 1. Introduction

Energy regulation problem has numerous applications in physics and engineering, such as energy harvesting [1,2], deployment of tethered systems [3], quantum control [4–6] and many other applications. An efficient approach to energy control is based upon the speed gradient (SG) method [7], resulting in the closed-loop system possessing a pre-specified positive function, which decreases along the system trajectories. In the series of papers, the SG method was extended to design energy regulation algorithms for spatially distributed systems, using the boundary and distributed control of spatially-distributed systems, see [7,8].

During the digitalization of mechatronic complexes under the condition of a deficiency of the available capacity of digital communication channels ensuring the information exchange in the complex, the problem can arise in ensuring the transmission of information necessary for observation and control between different components of the system, such as sensors, controlling devices, and actuators. An efficient approach to analyze systems robustness under disturbances caused by sampling is based on the time-delay method proposed by E. Fridman and coauthors [9,10]. The problem of information exchange is especially heavy for observation and control of spatially distributed plants described by

partial differential equations due to the complexity of their dynamics, a wide frequency band characterizing the processes in the system, the action of spatially distributed disturbances, and, in many cases, because of the need to use a large number of sensors and actuators located at considerable distances from the computing device. It is possible to facilitate the solution of observation and control problems under these conditions by using smart, including adaptive, sensors, in which measurement results are encoded for transmission via a digital communication channel to an appropriately designed decoder. Up to the authors' knowledge, there exist only a few results on robustness with respect to data sampling for parabolic PDE and hyperbolic Partial Differential Equations–Ordinary Differential Equations (PDE–ODE) loops, such as [11–17].

Proceeding from the previous studies of the Authors [8,17], this paper is devoted to the energy control for the sine-Gordon system. In recent years, this system has become earned significance as a model for investigations in nonlinear physics, see for example, [18–22]. This system demonstrates such nonlinear behavior as solitons, kinks, antikinks, and breathers, see [23–27] for mentioning a few, and also serves as the basis for modeling various physical processes, such as the propagation of an optical pulse in a waveguide [28], the transition from static to dynamic friction [29], spin dynamics of an anisotropic Heisenberg ferromagnetic chain [30], phase transition between the superfluid and the insulating ground states of the Bose-Hubbard [31], effects of Ohmic dissipation in Josephson junctions [18,32,33], dynamics of mechanical transmission lines, see [34–37].

Andrievsky et al. [17] numerically studied the SG-based state feedback energy control of [8] and the system robustness with respect to the data sampling. Properties of six algorithms, such as “proportional”, “relay”, “adaptive-relay”, and combinations thereof, according to such performance criteria as limiting error, transient time, and stability threshold with respect to the data sampling interval, are studied. It is found that for the problem under consideration, the simplest, proportional SG (P-SG) algorithm has an advantage. It should be noted that the mentioned above papers considered only the measured data sampling but did not take into account the constraints imposed on the data transfer rate over the communication channel; potentially, the number of bits transmitted at sampling (measurement) instants can be arbitrarily large there. In the present paper focused on the estimation and control of the energy for a distributed sine-Gordon system through limited capacity communication channels, the results of the [8,17] are extended. In contrast to [17], in this paper, as well as in [8], the feedback control is considered both by the full system state and by the measured output of the chain (and not only by the state), and the P-SG algorithm is used, which was not studied by Orlov et al. [8]. This paper develops the previous results of the Authors in the field of control of energy for spatially distributed systems. A difficult problem is one of minimizing the amount of information required for control. A step in this direction was made in [8], where the possibility of using not the entire distance vector of the chain and its time derivative (which have an infinite dimension), but by employing the state observer, only a small number of local measurements. When quantizing control processes, an important problem arises with minimizing the amount of information transmitted over a digital communication channel on which the present study is focused. To the best of the Authors' knowledge, there are currently no publications on the observation and control of nonlinear distributed chains through communication channels with limited capacity.

The applications of binary coding of output measurements by the first and full order coders/decoders pairs are considered, for each of which the use of time-invariant, and adaptive coding procedures are studied. The outputs are measured in the chain's separate sections and are used by the state Luenberger-type observer to estimate the inner state of the system at all points. The procedures for estimating the chain state over the limited capacity communication channels are presented. The comparative simulation results are presented, demonstrating the dependence of the estimation and control accuracy on the data transfer bitrate.

The main contribution of the paper is the development of data encoding/decoding procedures that minimize the data bit rate of the communication channel when controlling the energy of nonlinear distributed sine-Gordon chains. Four data transmission procedures are proposed and studied numerically, including combinations of first and full-order coding, time-invariant and adaptive. For each of them, the accuracy of not only state estimation but also controlling the system energy by output using an observer is examined. On the basis of the quantitative study, permissible limits for minimizing the load of the communication channel were revealed. The observation and control structures proposed in the paper can also be used for other types of spatially distributed systems.

The remainder of the paper is organized as follows. Section 2 is devoted to a controlled sine-Gordon system model description and an energy control problem statement. Continuous-time algorithms for state estimation and energy control are briefly recalled in Section 4. Section 3 is concerned with the problem of state estimation over the limited capacity digital communication channel. In this Section, the state observation scheme with data transferring over the communication channel is described, and the coding-decoding procedures for the system of interest are presented. Numerical examination results for various cases of the estimation, control, and communication schemes are described in Section 5 and consolidated in the tables at the end of this Section. Concluding remark and future work intentions of Section 6 finalize the paper.

## 2. Plant Model and Problem Statement

Let us briefly recall the key points of [8,17]. The following dissipation-free sine-Gordon system model is considered

$$x_{tt} = \kappa x_{rr} - F_0 \sin x + u(r, t), \quad t \geq 0, \quad (1)$$

where  $t \in \mathbb{R}$  denotes the time;  $r \in [0, 1]$  is the scalar spatial variable;  $x = x(\cdot, t)$  is the instant state of the system,  $x(r, t) : \mathbb{R}^2 \rightarrow \mathbb{R}$ ;  $\kappa, F_0$  are for system parameters;  $u(r, t)$  denotes the control input. In what follows, time  $t$  is conventionally measured in seconds, while other variables are assumed to be dimensionless. The following Dirichlet boundary conditions are stated for the PDE (1)

$$x(0, t) = 0, \quad x(1, t) = 0. \quad (2)$$

The following sampled-in-space actuation is used to control sine-Gordon model (1)

$$u(r, t) = \sum_{i=1}^m b_i(r) u_i(t) \quad (3)$$

which is, thus, representable in the form

$$x_{tt} = \kappa x_{rr} - F_0 \sin x + \sum_{i=1}^m b_i(r) u_i(t), \quad t \geq 0. \quad (4)$$

Such actuation is constituted by in-domain control channels, which are characterized by spatial distributions  $b_i(r) \in H^2$ ,  $i = 1, \dots, m$  of control inputs  $u_i(t)$ , located on disjoint actuator subdomains  $\text{supp } b_i(\cdot) \subseteq [r_i, r_i + h_i] \subseteq [0, 1]$  of some lengths  $h_i > 0$ . Recall that the Sobolev space  $H^l(a, b)$  with a natural index  $l$  consists of  $l$  times weakly differentiable functions  $x(r) : \mathbb{R} \rightarrow \mathbb{R}$ , which are defined on the domain  $(a, b) \subset \mathbb{R}$  and whose norm is given

by  $\|x(\cdot)\|_{H^l(a,b)} = \sqrt{\sum_{j=1}^l \int_a^b (\partial^j x / \partial r^j)^2 dr}$ . By default,  $H^0(a, b) = L_2(a, b)$  and  $H^l(0, 1) = H^l$ .

As in [8,17], the spatial domain  $[0, 1]$  is uniformly partitioned into  $m = 10$  subdomains  $[r_i, r_i + h_i]$  of lengths  $h_i = 0.1, i = 1, \dots, 10$  so that  $r_i = 0.1(i - 1)$ . Within each subdomain the corresponding actuator distribution  $b_i(r)$  is specified as

$$b_i(r) = \begin{cases} 1, & \text{if } r_i + 0.02 \leq r \leq r_i + 0.08, \\ 0, & \text{otherwise,} \end{cases} \tag{5}$$

i.e., the first and the last actuators are located in the distance 0.02 from the left and right boundaries, respectively, whereas the neighboring actuators possessed a slot of the length 0.04 between them.

Energy  $E(x, x_t)$  of sine-Gordon model (1), (2) is given by the following expression [7]

$$E(x, x_t) = \frac{1}{2} \int_0^1 (x_t^2 + kx_r^2 + 2F_0(1 - \cos x)) dr \tag{6}$$

The control objective is regulation the chain (1)–(3) energy  $E(x, x_t)$  to a prespecified level  $E_* \geq 0$  for guaranteeing the limiting relation

$$\lim_{t \rightarrow \infty} E(x(\cdot, t), x_t(\cdot, t)) = E_*. \tag{7}$$

### 3. Continuous-Time Algorithms for State Estimation and Energy Control

This section briefly provides preliminary information from [8,17] related to continuous-time state estimation and energy control without digitalization and data transmission over digital communication channels.

#### 3.1. Energy Control Synthesis Using State Feedback

##### 3.1.1. Basics of SG Design Method

Following [7], let us briefly outline the main points of the SG design methodology in the part that is used for the purposes of this paper.

Consider the following controlled plant model

$$\dot{x}(t) = f(x, \theta, t), \tag{8}$$

where  $x(t) \in \mathbb{R}^n$  denotes the state vector;  $\theta(t) \in \mathbb{R}^m$  is the control vector;  $f(\cdot)$  is a certain vector-function continuous in  $x, \theta, t$ , and continuously differentiable in  $\theta$ .

Let the “admissible control laws” be of the form

$$\theta(t) = \Theta(\{x(s)_{s=0}^t\}, \{\theta(s)_{s=0}^t\}) \tag{9}$$

with some operator  $\Theta$ , such that the solutions of the system (8), (9) exist and are unique for  $t \geq 0$  for any initial values  $x_0, \theta_0$ .

Let the control goal be expressed by the asymptotic relation

$$\lim_{t \rightarrow \infty} Q_t = 0. \tag{10}$$

where  $Q_t = Q(\{x(s)_{s=0}^t\}, \{\theta(s)_{s=0}^t\})$  is a given (local) objective functional

$$Q_t = Q(x(t), t), \quad Q(\cdot) \in \mathbb{R}, \tag{11}$$

The SG algorithm in its finite form is as follows:

$$\theta(t) = -\psi(x, \theta, t), \tag{12}$$

where  $\Gamma = \Gamma^T > 0$  stands for  $m \times m$ -matrix of algorithm gains;  $\omega(x, \theta, t)$  denotes derivative of the objective functional along system (8) trajectories;  $\psi(x, \theta, t)$  is a certain vector-function satisfying the following “pseudogradient condition”:

$$\psi(x, \theta, t)^T \nabla_{\theta} \omega(x, \theta, t) \geq 0. \tag{13}$$

The exact formulations can be found in ([7], Section 2.1).

In the present study function

$$\psi(x, \theta, t) = \Gamma \nabla_{\theta} \omega(x, \theta, t) \tag{14}$$

is employed, where  $\Gamma$  is a diagonal matrix,  $\Gamma = \gamma \mathbf{I}_{m \times m}$ , and  $\gamma$  is the proportional controller gain.

### 3.1.2. SG Energy Control Law in Proportional Form

Following the SG design procedure [7], introduce the goal functional as

$$Q(t) = \frac{1}{2} (E(t) - E_*)^2. \tag{15}$$

Then compute the time derivative of  $Q(t)$  along the system (1), (2) trajectories, provisionally assuming that  $u(r, t)$  is constant on  $t$ . Differentiating (15) in time, integrating then the resulting equality by part, and employing a consequence  $x_t(0, t) = x_t(1, t) = 0$  of the boundary condition (2) yield

$$\dot{Q} = (E(t) - E_*) \int_0^1 u(r, t) \cdot x_t dr. \tag{16}$$

The control action in [8,17] is specified in the form of a finite number of sampled-in-space actuators (3). Then  $\dot{Q}$  reads as

$$\dot{Q} = (E(x, x_t) - E_*) \sum_{i=1}^m \left( u_i(\cdot) \int_{r_i}^{r_i+h_i} b_i(r) x_t dr \right). \tag{17}$$

At the second step of the SG procedure, one should derive the gradient  $\nabla_u \dot{Q} \in \mathbb{R}^m$  of the resulting expression of  $\dot{Q}$  with respect to the control components  $u_i(t), i = 1, \dots, m$ , thus, arriving at

$$\nabla_u \dot{Q} = (E(x, x_t) - E_*) \begin{bmatrix} \int_{r_1}^{r_1+h_1} b_1 x_t dr & \dots & \int_{r_m}^{r_m+h_m} b_m x_t dr \end{bmatrix}^T.$$

This leads to the following sampled-in-space actuation (3) in Proportional form

$$u_i(t) = \gamma \Delta E(t) \int_{r_i}^{r_i+h_i} b_i x_t dr, \tag{18}$$

where the energy error  $\Delta E(t) = E_* - E(x, x_t)$  is introduced,  $i = 1, \dots, m$ ;  $\gamma$  is the positive controller gain (the design parameter). This parameter is chosen by the developer when synthesizing the control algorithm. As follows from the SG method (see Section 3 above and [7]), as well as the proof for the relay-type algorithm of [8], theoretically, any positive value of  $\gamma$  leads to the achievement of the control goal. However, as is usually the case in the synthesis of control systems, the designer can use additional criteria and conditions for the operation of the system, so the choice of  $\gamma$  is usually associated with some compromise. For example, as demonstrated in ([8], Figure 10), under state feedback control (18), the time of the transient process of establishing the given energy decreases monotonically as  $\gamma$  rises

to a certain value. However, under the output control (25), this process stops at the smaller value of  $\gamma$ . Indeed, there exists an observer dynamical error at the beginning of the process, and the high-speed controller then works at the beginning based on incorrect information about the controlled variable. For this article, the authors chose for each channel, value  $\gamma_i = 22.8$  as in [17].

Andrievsky et al. [17] considered some more SG energy control laws.

### 3.2. Sine-Gordon Chain State Estimation

#### 3.2.1. Sampled-in-Space Sensing

Following [8], the available position sensing of the sine-Gordon boundary-value problem (4), (2) is assumed to be of the form

$$y_j(t) = \int_0^1 x(r,t)\varphi_j(r)dr, \quad j = 1, \dots, l. \tag{19}$$

Note that in this paper, the simplified form of the observer by Orlov et al. [8] is used, where only position, not the velocity, sensors are employed.

The in-domain measurements (19) are characterized by the sensor spatial distribution  $\varphi_j(r) \in H^2$  with disjoint sensor locations

$$\text{supp } \varphi_j(\cdot) \subseteq [r_j^\varphi, r_j^\varphi + h_j^\varphi] \subseteq [0, 1], \quad j = 1, \dots, l. \tag{20}$$

These locations are introduced in a manner similar to the actuator subdomains (5). Although the sensors are not in general collocated to the actuators, however, the output feedback synthesis to be developed relies on the collocated sensing and actuation such that

$$\varphi_j(r) \equiv b_{i_j}(r), \quad j = 1, \dots, l \quad \text{for some } i_j \in \{1, \dots, m\}. \tag{21}$$

#### 3.2.2. Luenberger-Type Observer

For the position and velocity estimates  $\tilde{\zeta}(r, t)$  and  $\zeta(r, t)$  of the state components  $x(r, t)$  and, respectively,  $x_t(r, t)$  of the sine-Gordon model (1), (2), the following Luenberger-type observer is proposed and studied in [8]:

$$\tilde{\zeta}_t = \zeta + \sum_{j=1}^l \mu_j \varphi_j(r) \left( y_j(t) - \int_0^1 \varphi_j(\rho) \tilde{\zeta}(\rho, t) d\rho \right) \tag{22}$$

$$\zeta_t = \kappa \tilde{\zeta}_{rr} - F_0 \sin \zeta + u(r, t) \tag{23}$$

where  $\mu_j \geq 0$  are observer gains,  $\varphi_j(r)$  denote the identical weighted functions of the position sensor locations (20),  $j = 1, \dots, l$ . As one can see, following the Luenberger approach, observer (22), (23) mimics the structure of the estimated model, separately given for the canonical position-velocity variables  $x$  and  $x_t$ . Then, the observer PDEs (22), (23) are subjected to the Dirichlet boundary conditions  $\tilde{\zeta}(0, t) = 0, \tilde{\zeta}(1, t) = 0$ .

#### 3.2.3. Output Feedback Control of Sine-Gordon Chain Energy

For output feedback energy control of the sine-Gordon chain, the following control law is suggested, where instead of  $x, x_t$  in (6), (18) the estimates  $\tilde{\zeta}, \zeta$ , obtained by the observer (22), (23) are employed:

$$\hat{E}(\xi, \zeta) = \frac{1}{2} \int_0^1 (\zeta^2 + k\zeta_r^2 + 2F_0(1 - \cos \xi)) dr \tag{24}$$

$$u_i(t) = \gamma \Delta \hat{E}(t) \int_{r_i}^{r_i+h_i} b_i \zeta dr, \tag{25}$$

where the estimated energy error  $\Delta \hat{E}(t) = E_* - \hat{E}(\xi, \zeta)$  is introduced,  $i = 1, \dots, m$ ;  $\gamma$  denotes the positive controller gain. In summary, the proposed output feedback energy control law is described by (3), (22)–(25).

In [8], the estimation error dynamics and their well-posedness are studied, and the output feedback control by means of SG relay algorithm, using sampled-in-space sensing and actuation is examined both analytically and numerically.

**Remark 1.** *It should be mentioned that, compared with state feedback control, output feedback control has obvious disadvantages associated with the occurrence of additional dynamic errors associated with the transient process of state estimation using an observer, as well as errors caused by the uncertainty of the plant parameters (in the case under consideration, these are the parameters  $\kappa, F_0$ ). Typically, when controlling distributed systems, approximation of PDEs by ODEs, based on expansion in terms of eigenfunctions, the Galerkin method, or model reduction, is performed [11,38]. However, since the energy of the chain, according to (6), is defined via  $x(r, t)$  and  $x_t(r, t)$ , and it is practically impossible to measure these variables themselves, the use of the state observer seems to be the only practically implementable way to control. The impact of parametric uncertainty can be reduced by using adaptive estimation methods, the consideration of which is beyond the scope of this paper.*

The present paper is focused on algorithm design and studying the observation and control of the chain energy for the case of the measurements transmitting over limited-capacity digital communication channels. The rest of the Sections are concentrated on this topic.

#### 4. State Estimation over the Digital Communication Channel

##### 4.1. Observation Scheme with Transferring Data over the Communication Channel

Let the in-domain measurement signals  $y_j(t)$ ,  $j = 1, \dots, l$ , see (19), be transmitted over the limited capacity communication channel. In the present study, we assume that control action  $u(r, t)$ , see (3), is perfectly known at the receiver side. and the communication channel is ideal, although introduces time and level quantization to transmitted data. Let us further assume that the sampling occurs with some constant period  $T_s$ . Let us denote the sampling times as  $t_k = kT_s$ , where  $k \in \mathbb{Z}$  is the iteration number (the “discrete time”). Thus, a sequence of discrete-time signals  $y_j[k] = y_j(t_k)$ ,  $j = 1, \dots, l$  is applied to the coder for transmitting over the channel to the receiver side (hereinafter, square brackets are used for the argument of discrete-time processes). At instants  $t_k$ , the decoder produces the restored signals  $\bar{y}_j[k]$  for each transmitter channel. In this study, it is adopted that on the receiver side, the zero-order extrapolator is used to convert the discrete-time signals  $\bar{y}_j[k]$  to the continuous time ones,  $\bar{y}_j(t)$  such that  $\bar{y}_j(t) = \bar{y}_j[k]$  as  $t_k \leq t < t_{k+1}$ . Taking this into account, the following observer equations are derived by replacing  $y_j(t)$  with  $\bar{y}_j(t)$  in (22), (23):

$$\xi_t = \zeta + \sum_{j=1}^l \mu_j \varphi_j(r) (\bar{y}_j(t) - \int_0^1 \varphi_j(\rho) \xi(\rho, t) d\rho) \tag{26}$$

$$\zeta_t = \kappa \zeta_{rr} - F_0 \sin \xi + u(r, t). \tag{27}$$

#### 4.2. Coding-Decoding Procedures

##### 4.2.1. Time-Invariant Coder of First Order

Consider transmission of the signal over the digital communication channel, where both time-sampling and level quantization procedures are present. Let us consider the binary coder with memory, cf. [39–47].

Let signal  $y(t)$  be transmitted over the digital communication channel at sampling instants  $t_k = kT_s$ , where  $T_s > 0$  is a constant sampling period,  $k = 0, 1, \dots$  are integers. At each  $k$ , the deviation signal  $\delta[k]$  between transmitted signal  $y(t_k)$  and a certain centroid  $c[k]$  (given below by (29)) is calculated as  $\delta[k] = y(t_k) - c[k]$ . Signal  $\delta[k]$  is subjected to the following binary quantization scheme:

$$\bar{\delta}[k] = M \text{sign}(\delta[k]). \tag{28}$$

where  $\text{sign}(\cdot)$  is signum function,  $M > 0$  may be referred to as a quantizer range. Then the quantizer output  $\bar{\delta}[k]$  is coded by the available binary alphabet  $\Sigma = \{-1, 1\}$  and, in the form of the binary signal  $\sigma \in \{-1, 1\}$ ,  $\sigma[k] = \text{sign}(\delta[k])$  is transmitted over the communication channel to the decoder. The sequence of central numbers  $c[k]$  is recursively defined by the following algorithm:

$$c[k + 1] = c[k] + M\sigma[k], \quad c[0] = 0. \tag{29}$$

Evaluating an upper bound of data transmission error  $d(t)$  can be made under the assumption that it is known the exact bound  $L_y$  for the rate of  $y(t)$  is  $L_y = \sup_{x \in \Omega} |C\dot{x}|$ , where  $\dot{x}$  is from (1). Let us define  $\Delta = \sup_t |d(t)|$ . From (28)–(35) follows that for  $t \in [t_k, t_{k+1})$ , the transmission error is as  $d(t) = y(t) - c(t)$ , where  $c(t) = c[k]$ . From the coding-decoding scheme (28)–(35) it is clear that for each time interval  $t \in [t_k, t_{k+1})$ , the transmission error may be represented as  $d(t) = y(t) - c(t)$ , where  $c(t) = c[k]$ . To evaluate  $|\delta[k]|$ , assume that for a certain  $k$  is valid that

$$|y(t_k) - c[k - 1]| \leq 2M. \tag{30}$$

Due to the assumption on  $y(t)$  rate limitation, over the each time interval  $t \in [t_k, t_{k+1})$  the magnitude of  $d(t)$  is bounded by  $|\delta(t)| + L_y T$ , where  $\delta(t) = \delta[k]$  as  $t \in [t_k, t_{k+1})$ . Then, after renovation of  $c$  by means of (35), at step  $k$  is valid that the magnitude of error  $\delta[k] = y(t_k) - c[k]$  does not exceed  $M$ . Therefore, the magnitude of  $d(t)$  is bounded by  $|\delta(t)| + L_y T_s$ , where  $\delta(t) = \delta[k]$  as  $t \in [t_k, t_{k+1})$ , and after renovation of  $c$  by means of (35), at step  $k$  it is valid, that  $\delta[k] = y(t_k) - c[k]$  does not exceed  $M$ .

This leads to the following inequality

$$\Delta < M + L_y T_s. \tag{31}$$

If  $M$  is chosen, satisfying the condition

$$M > L_y T_s, \tag{32}$$

then at instant  $t_{k+1}$  inequality (30) will be fulfilled, and the aforementioned relation will be recursively valid for  $k := k + 1$  and, using the mathematical induction argument, for all consequent steps.

Inequality (32) imposes restrictions on sampling period  $T$  and quantizer range  $M$  for a given growth rate  $L_y$  of  $y(t)$ . If (32) is fulfilled, then magnitude  $|d(t)|$  of data transmission error  $d(t)$  does not exceed  $\Delta$ . Otherwise, the data transmission scheme based on (28)–(34)

can fail in the sense that the data transmission error for several steps can be greater than the prescribed bound  $\Delta$ . Therefore, it is reasonable to choose  $M$  as

$$M = \alpha L_y T_s, \tag{33}$$

where a certain design parameter  $\alpha > 1$  is chosen.

Equations (28) and (29) describe the coder algorithm. A similar algorithm is represented by the decoder: values of  $\bar{\delta}y[k]$  are restored with given  $M$  from the received binary codeword  $\sigma[k]$  as  $\bar{\delta}y[k] = M\sigma[k]$ . Then the decoder output  $\bar{y}[k]$  is found as

$$\bar{y}[k] = \bar{c}[k] + \bar{\delta}y[k]. \tag{34}$$

Centroid  $\bar{c}[k]$  is recursively found at the decoder side in accordance with (29):

$$\bar{c}[k + 1] = \bar{c}[k] + M\sigma[k], \quad \bar{c}[0] = 0. \tag{35}$$

**Remark 2.** Obviously, the smaller parameter  $M$  is, the smaller the data transmission error, but the inequality (32) limits the minimum value of  $M$ . This issue is discussed in the framework on the “zooming” concept, cf. [39,41,48] and in the adaptive coding procedure described in Section 4.2.3 below.

**Remark 3.** Since the binary coder (28) is used, then this coding scheme corresponds to the channel data transmission rate as  $R = T_s^{-1}$  bits per second.

#### 4.2.2. Time-Invariant Coder of Full Order

The idea behind the full-order coding procedure is as follows. The coder incorporates the “embedded” observer, cf. [41,48–50]. On the encoder side, the measured sampled data are quantized by the level according to the chosen (say, binary) quantization procedure and fed to the observer, whose structure corresponds to the complete model of the controlled plant. The peculiarity is that although on the encoder side, the measurement results are considered known and not level quantized, the quantization procedure is implemented in relation to the measurement signals to ensure the so-called equi-memory condition [41], which requires that both the encoder and the decoder should work based on the same information. Further, the update (residual) signal of the observer on the encoder side is transmitted in a quantized form through the communication channel and is used to correct a similar observer included in the decoder. Its state variables are used further as estimates of the plant state. Potentially, such a scheme makes it possible, at a sufficiently high communication channel capacity, asymptotically in time, vanishing the state estimation error.

Let us describe an implementation of this approach to the considered problem of the sine-Gordon chain (1), (2) state estimation. The observer, embedded in the coder, is represented by

$$\xi_t = \zeta + \sum_{j=1}^l \mu_j \varphi_j(r) \bar{\varepsilon}_j(t) \tag{36}$$

$$\zeta_t = \kappa \zeta_{rr} - F_0 \sin \xi + u(r, t). \tag{37}$$

where  $\bar{\varepsilon}_j(t)$  are generated for  $j = 1, \dots, l$  by the binary coding procedure (28), (29), applied to the mismatch signals  $\varepsilon_j(t) = y_j(t) - \int_0^1 \varphi_j(\rho) \xi(\rho, t) d\rho$ . More specifically,  $\varepsilon_j(t)$  are taken instead of  $y_j(t)$  in (28), (29), which leads to the following coding procedure: the deviation signals  $\delta_j[k]$  between transmitted signal  $\varepsilon_j(t_k)$  corresponding centroids  $c_j[k]$ , given by (29),

are calculated as  $\delta_j[k] = \varepsilon_j(t_k) - c_j[k]$ . Then the binary quantization scheme (28) is applied to  $\delta[k]$  and signals  $\bar{\varepsilon}_j(t)$  are formed as

$$\bar{\varepsilon}_j[k] = M \operatorname{sign} \delta_j[k], \quad j = 1, \dots, l. \tag{38}$$

The binary-valued signals  $\sigma_j[k] \equiv \operatorname{sign} \delta_j[k]$  are transferred to the receiver over the communication channel at instants  $t_k = kT_s$ . On the receiver side, the values of  $\bar{\varepsilon}_j$  are restored with given  $M$  from the received binary codeword  $\sigma[k]$  as  $\bar{\varepsilon}_j = M\sigma_j[k]$ . Then the decoder output  $\bar{y}_j[k]$  is found as

$$\bar{\varepsilon}_j[k] = \bar{c}_j[k] + M\sigma_j[k]. \tag{39}$$

The receiver’s centroids  $\hat{c}[k]$  are found as follows

$$\hat{c}_j[k + 1] = \hat{c}_j[k] + M\sigma_j[k], \quad \hat{c}_j[0] = 0, \quad j = 1, \dots, l. \tag{40}$$

The observer, embedded in the receiver, is also used as the system state estimator. It is governed by the algorithm, similar to one on the coder’s side, with the exception that the correction (renovation) signals  $\bar{\varepsilon}_j(t)$  are obtained by the zero-hold extrapolation on sampling period  $T_s$  of signals  $\bar{\varepsilon}[k]$ , which are received over the communication channel:

$$\hat{\zeta}_t = \hat{\zeta} + \sum_{j=1}^l \mu_j \varphi_j(r) \bar{\varepsilon}_j(t) \tag{41}$$

$$\hat{\zeta}_t = \hat{\kappa} \tilde{\zeta}_{rr} - F_0 \sin \hat{\zeta} + u(r, t). \tag{42}$$

Summarizing, in the proposed full-order coding/decoding scheme, the innovation signals  $\bar{\varepsilon}_j[k]$  are transmitted over the channel, govern the observer on the decoder side, and  $\hat{\zeta}$  and  $\tilde{\zeta}$  are used as the plant position and velocity estimates.

#### 4.2.3. Adaptive Coding

In time-varying quantizers [41,45,48,51,52] range  $M$  is updated with time. Using such a zooming strategy improves the steady-state accuracy of the transmission procedure and, at the same time, prevents the encoder saturation during the process beginning. The values of  $M[k]$  may be precomputed (the time-based zooming), or current quantized measurements may be used at each step for updating  $M[k]$  (the event-based zooming). For an audio channel, Moreno-Alvarado et al. [53] developed the coding schemes with the capacity to simultaneously encrypt and compress audio signals, which makes the possible increasing necessity for transmitting sensitive audio information over insecure communication channels.

The event-based zooming can be realized in the form of adaptive zooming, see [48,54,55], where the quantizer’s range is adjusted automatically depending on the current variations of the transmitted signal.

For the binary quantizer, the following adaptive zooming algorithm was proposed and experimentally studied in [48]:

$$\lambda[k] = (s[k] + s[k - 1] + s[k - 3])/3, \quad s[-1] + s[-2] = 0,$$

$$M[k + 1] = m_c + \begin{cases} \rho M[k], & \text{if } |\lambda[k]| \leq 0.5, \\ M[k]/\rho, & \text{else,} \end{cases} \tag{43}$$

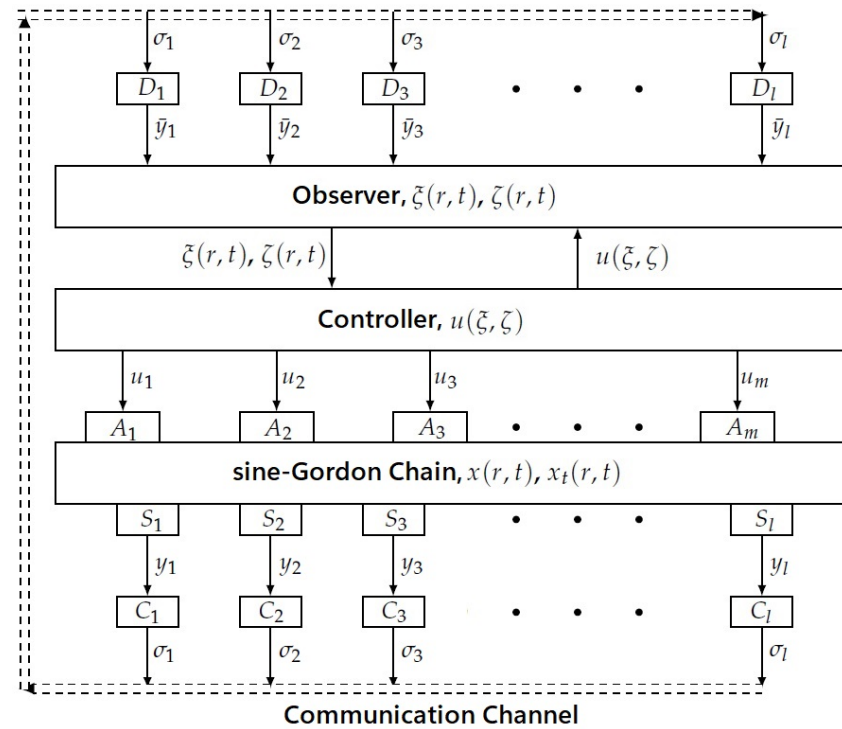
$$\bar{\sigma}[k] = M[k]s[k],$$

where  $M[0] = M_0$  is an initial value of  $M[k]$  (the design parameter);  $\bar{\sigma}[k]$  denotes the value of  $\sigma[k]$  recovered at the decoder side from binary values  $s[k]$ . Unlike the case of time-based zooming, the initial value  $M_0$  can be chosen in the wide range since  $M[k]$  is automatically

adjusted and can be increased or decreased during the zoom-in and zoom-out stages. The decay parameter  $0 < \rho \leq 1$  serves for setting the rate of change of the quantization range  $M[k]$ .

This adaptive coding procedure can be applied both for the first-order and the full-order communication schemes. In the first case, the sensors measurements  $y_j(t), j = 1, \dots, l$ , are coded and transmitted over the channel (see Section 4.2.1); in the second one, the adaptive coding procedure is applied to innovation signal  $\varepsilon(t)$ , as described in Section 4.2.2.

The overall block diagram of the control system (3), (22)–(25) with data transmission via the communication channel is depicted in Figure 1.



A—actuator, S—sensor, C—coder, D—decoder

Figure 1. Block diagram of control system (3), (22)–(25) with data quantization.

**Remark 4.** The closed-loop system stability was theoretically studied in the previous authors' works. In ([8], Theorem 2), the closed-loop system with the state feedback (1), (6), (18) stability has been proved for a similar to (18) algorithm with the only difference that the error signum-wise gain has been used instead of the present linear gain in (18). However, the line of reasoning remains applicable for the stability proof in the present case as well. Regarding the stability of the system with the observer-based output feedback control described by (3), (22)–(25) ([8], Theorem 4) proved the convergence of the observer and the output feedback case. In ([8], Theorem 5) is proved locally for the non-linear sine-Gordon chain, and state feedback stabilization of the corresponding invariant manifold has been globally proved. With this in mind, the detailed stability proof is skipped since it is beyond the scope of the present paper, which is focusing on the numerical shreds of evidence supporting the closed-loop stability in the control-quantified setting.

To the best Authors' knowledge, up to now on, there are no publications on the control of nonlinear spatially distributed systems over communication channels with limited bandwidth. A complete and rigorous analytical study of the stability of such systems is hardly possible, although there are numerous theoretical results for finite-dimensional systems, cf. [45,50,51,56–60]. In particular, [48,54,55,61] present the results of analytical and experimental studies on adaptive data coding during transmission over a digital communication channel in control systems. Due to the fact that the Lipschitz constant  $L_y$  differs in various areas of the system state, the justification of the stability of control systems with coding can only be local. Under these conditions, when there is no

universal solution covering all possible situations, intensive computer investigations are needed for designing a particular system.

**Remark 5.** The approach presented in this paper can be used not only for the sine-Gordon system under consideration but also for other systems whose dynamics are described by PDEs, including aerospace applications, cf. [62–64]. The closest problem to the one considered in this paper was studied by Gao and Liu [65], who had taken into account quantization by the level of control actions in constructing a neural network algorithm for suppressing elastic oscillations of the wing. As a direction for the development of the distributed systems control method described in this study, it seems promising and expedient to use optimal and adaptive-optimal control methods, among which it is worth highlighting the recent results on fuzzy optimal tracking control via single-network adaptive critic design. For example, in [66], almost optimal servo controllers for hypersonic aircraft are proposed, where the controllers for the velocity and the flight altitude subsystems are developed using brief fuzzy approximations, and then optimal controllers are implemented using adaptive critical design. The possibility of obtaining satisfactory performance for real-time systems is shown. Bu et al. [67] proposed a direct non-affine tracking control method, in which neural networks with fuzzy wavelets are used to build action networks and critic networks, and new direct non-affine controllers are proposed. To achieve the desired performance in a transient and steady state, Ref. [67] imposes behavioral restrictions on speed and altitude tracking errors.

### 5. Numerical Examination Results

In the simulations the following model (1) parameters are taken:  $J = 1, \kappa = 0.12, F_0 = 25$ . The initial states were pre-specified in the form

$$x(0, r) = A(1 - \cos(2\pi r))^7, \quad x_t(0, r) = 0 \tag{44}$$

with a “magnitude” parameter  $A = 0.03$ .

As in [17], control gains  $\gamma_i, i = 1, \dots, 10$  were set to  $\gamma_i = 22.8$  and the desired energy level was taken as  $E_* = 5$ . Number  $N = 2500$  was selected for the PDEs (1) to discretize the spatial variable  $r$  and duration of the computation time  $t_{\text{fin}}$  was confined to 30 s. Initial values of observers (26), (27), (41), and (42) states  $\xi, \zeta,$  and  $\hat{\xi}, \hat{\zeta}$ , respectively, are set to zero.

#### 5.1. Quality Indices

From the point of view of the authors, there is no single function (functional) of quality that would fully and comprehensively characterize the properties of the system. Therefore, as in [17], this article uses several functionals that reflect various aspects of system performance. They are as follows.

1. Based on [8], the following integral-quadratic function  $V(t)$  is used to evaluate the state observation estimation accuracy

$$V(t) = \frac{1}{2} \int_0^1 \left( F_0(\Delta \xi)^2 + \kappa(\Delta \xi_r)^2 + (\Delta \xi_t)^2 \right) dr, \tag{45}$$

where  $\Delta \xi(x, t) = \xi(r, t) - x(r, t)$ , and  $\Delta \xi_t(x, t) = \xi_t(r, t) - x_t(r, t)$ .

2. Since  $V(t)$  is a function, not a number, then, following the lines of [17], the corresponding quality functionals are introduced as:

- (a) its terminal value  $V(t_{\text{fin}})$ , where  $t_{\text{fin}}$  denotes the simulation time ( $t_{\text{fin}} = 30$  s in what follows);
- (b) transient time  $t_{\text{tr}}^V$ , understood as the maximal instant such that  $V(t) \geq 0.01V(0)$ . In the case of  $t_{\text{tr}}^V \geq 30$ , or does not exist, then  $t_{\text{tr}}^V$  is set to  $t_{\text{tr}}^V = \infty$ ;

3. Sine-Gordon chain energy  $E(x, x_t)$  given by (6) as

$$E(t) = \frac{1}{2} \int_0^1 \left( x_t^2 + kx_r^2 + 2F_0(1 - \cos x) \right) dr$$

4. The corresponding functionals are:

- (a)  $\Delta E(t) = E_* - E(t)$  terminal value  $\Delta E(t_{fin})$ ;
- (b) transient time  $t_{tr}^E$ , understood as the maximal instant such that  $\Delta E(t) \geq 0.01\Delta E(0)$ . If this instant is greater than  $t_{fin}=30$ , or the given condition does not happen at all, then the quality index is set to  $t_{tr}^E = \infty$ .

In the following sections, the values of the specified quality indices are established by modeling for the specified chain parameters, initial conditions, and the required energy value for various data encoding-decoding schemes.

### 5.2. Ideal Channel Case

This subsection is aimed to present the simulation results of the “ideal channel case” for comparatively demonstrating the impact of limited communication capabilities on the performances of state estimation and control procedures. No quantization is assumed here in the communication channel, except for the sampling of measurement data during the transmission of the output signal with the sampling time  $T_s = 1/400$  s.

#### 5.2.1. Free Motion State Estimation in Ideal Channel Case

The simulation results for free motion state estimation over the sampled-data communication channel with  $T_s = 1/400$  s and absence of the level quantization are depicted in Figures 2–4. The control action  $u(r, t)$  is taken equal to zero. Time history of  $V(t)$  and the spatiotemporal plot of the observer (22), (23) correction signal defined as

$$u_{obs}(r, t) = \sum_{j=1}^l \mu_j \varphi_j(r) \left( y_j(t) - \int_0^1 \varphi_j(\rho) \xi(\rho, t) d\rho \right), \quad j = 1, \dots, 5, \quad (46)$$

are plotted in Figure 2. The observer transient time as  $t_{tr}^V = 5.42$  s is found based on the initial value  $V(0) = 82.1$  and the threshold, calculated as  $0.01V(0)$ .

One can get an impression of the state estimation accuracy from Figure 3, where the time histories of  $x(0.5, t)$ ,  $\xi(0.5, t)$ , estimation error  $x(0.5, t) - \xi(0.5, t)$ , and  $x(0.75, t)$ ,  $\xi(0.75, t)$ ,  $x(0.75, t) - \xi(0.75, t)$  for  $t \in [0, 10]$  are depicted.

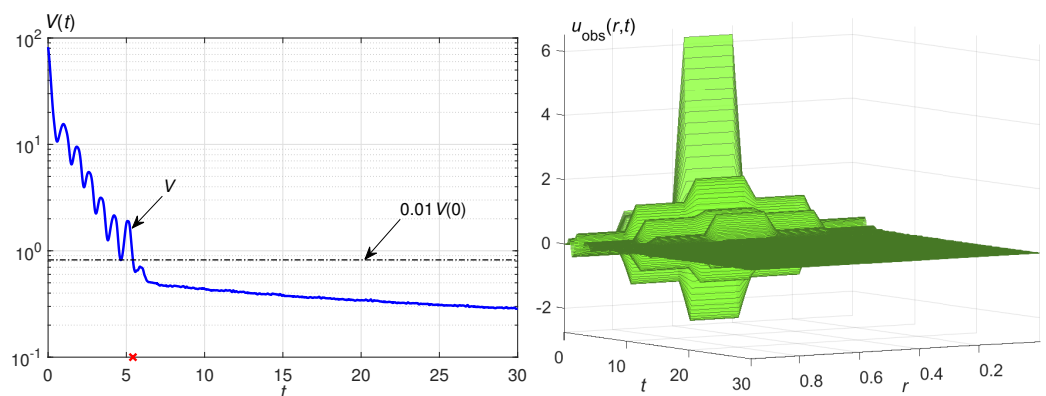


**Figure 2.** State estimation. Free motion case,  $u(r, t) \equiv 0$ , ideal channel.  $V(t)$  time history (left plot);  $u_{obs}$  spatiotemporal plot (right plot). Cross sign “x” marks  $t_{tr}^V$ .

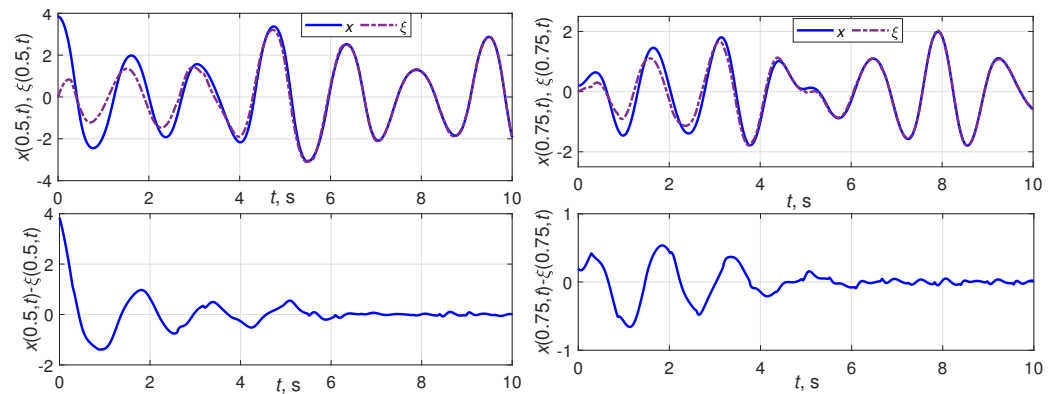


**Figure 3.** State estimation. Free motion case,  $u(r, t) \equiv 0$ , ideal channel.  $x(r, t), \xi(r, t), x(0.r, t) - \xi(r, t)$  time histories for  $r = 0.5$  (left column), and  $r = 0.75$  (right column).

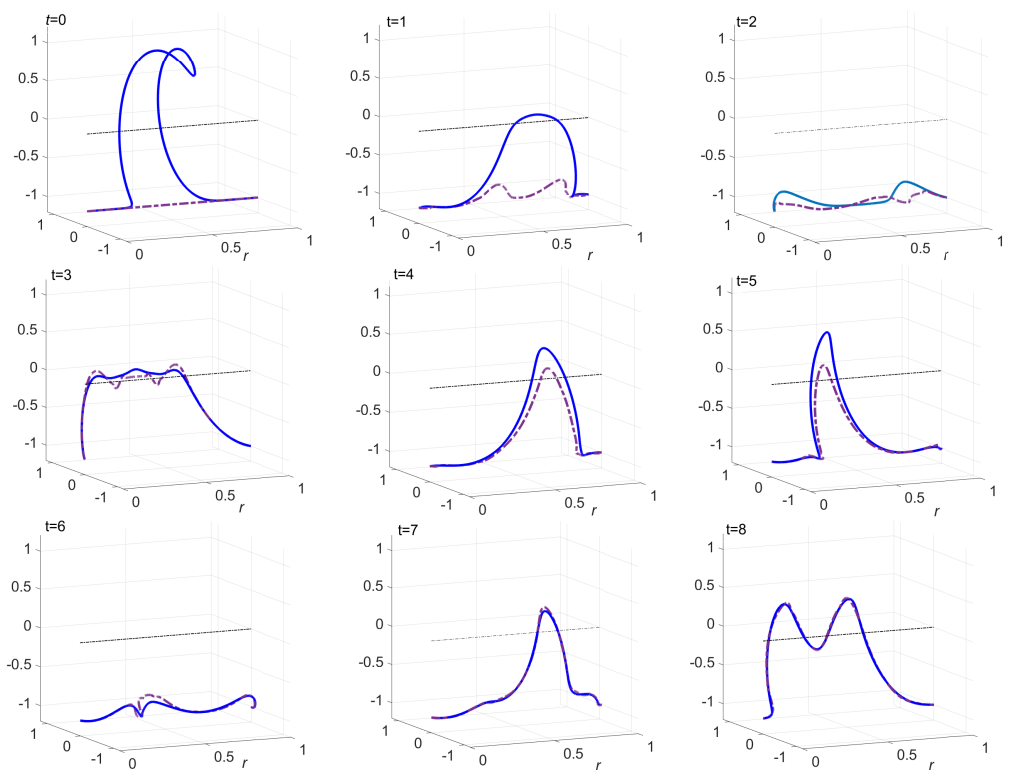


**Figure 4.** State estimation. Free motion case,  $u(r, t) \equiv 0$ , ideal channel. The visual representation of the system behavior and its state estimation process.

### 5.2.2. State-Feedback Control in Ideal Channel Case

The simulation results for the closed-loop energy control of the system, defined by (1), (2), (6), and (18) are demonstrated in Figures 5–8. The controller uses the state feedback; the state estimation process is performed over the sampled-data communication channel with  $T_s = 1/400$  s without the level quantization of measurements. This process does not have any effect on the controller behavior. Control action  $u(r, t)$  is assumed to be accurately known to the observer.

Time histories of  $E(t), V(t)$ , and the spatiotemporal plots of control signal  $u(r, t)$  and observer (22), (23) correction signal  $u_{obs}(r, t)$ , defined by (46), are plotted in Figures 5 and 6, respectively. The transient time for an energy control as  $t_{tr}^E = 1.04$  s is found based on the initial value  $\Delta E(0) = -15.7$  and the threshold, calculated as  $0.01\Delta E(0)$ . The observer transient time as  $t_{tr}^V = 2.39$  s is found based on the initial value  $V(0) = 82.1$  and the threshold, calculated as  $0.01V(0)$ . The finite values for  $t_{fin} = 30$  s are found as  $\Delta E(t_{fin}) = -3.30 \times 10^{-5}$ ,  $V(t_{fin}) = 0.32$ .

Figure 7, where the time histories of  $x(0.5, t)$ ,  $\xi(0.5, t)$ , estimation error  $x(0.5, t) - \xi(0.5, t)$ , and  $x(0.75, t)$ ,  $\xi(0.75, t)$ ,  $x(0.75, t) - \xi(0.75, t)$  for  $t \in [0, 10]$  are depicted, demonstrates the state estimation accuracy.

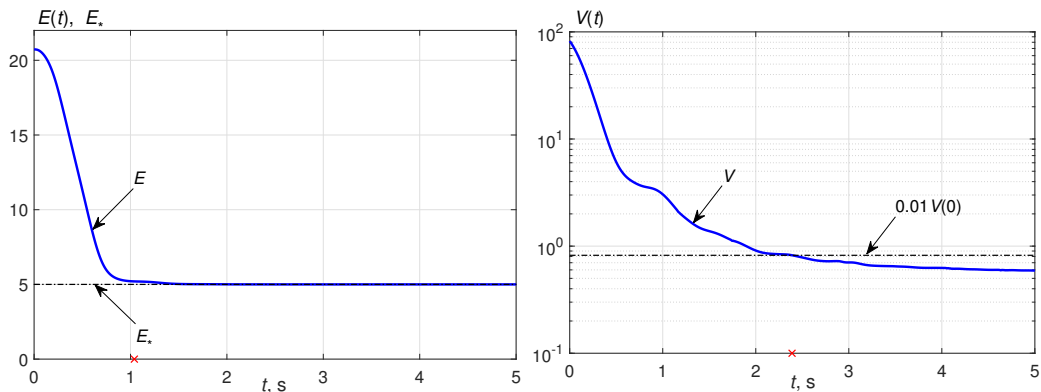


Figure 5. Feedback energy control (6), (18), ideal channel. Energy  $E(t)$  (left plot) and function  $V(t)$  (right plot) time histories. Cross sign “x” marks  $t_{tr}^E$  (left); Cross sign “x” marks  $t_{tr}^V$  (right).

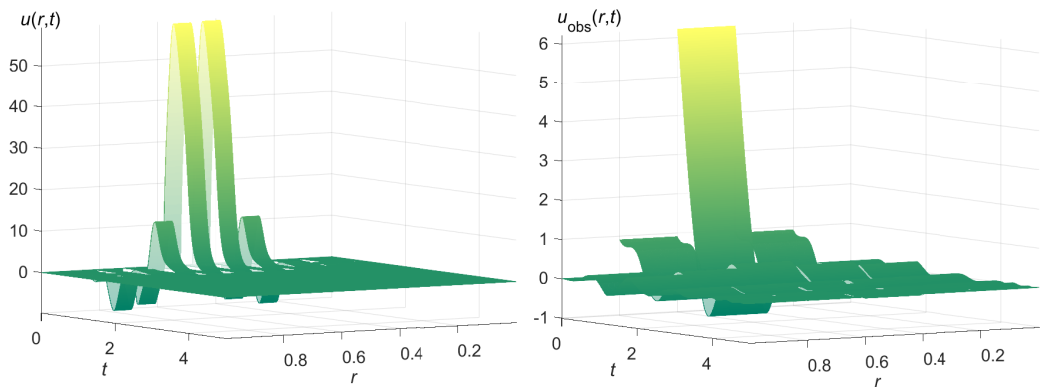


Figure 6. Feedback energy control (6), (18), ideal channel. Spatiotemporal plots of control signal  $u(r, t)$  and observer correction signal  $u_{obs}(r, t)$ .

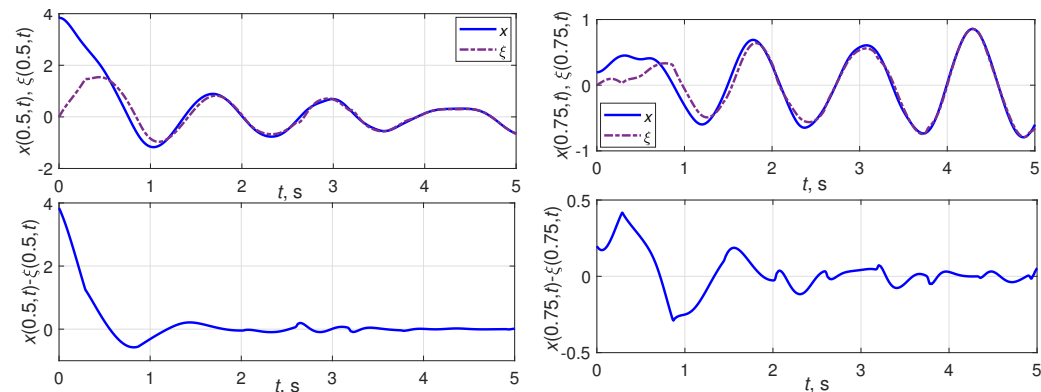
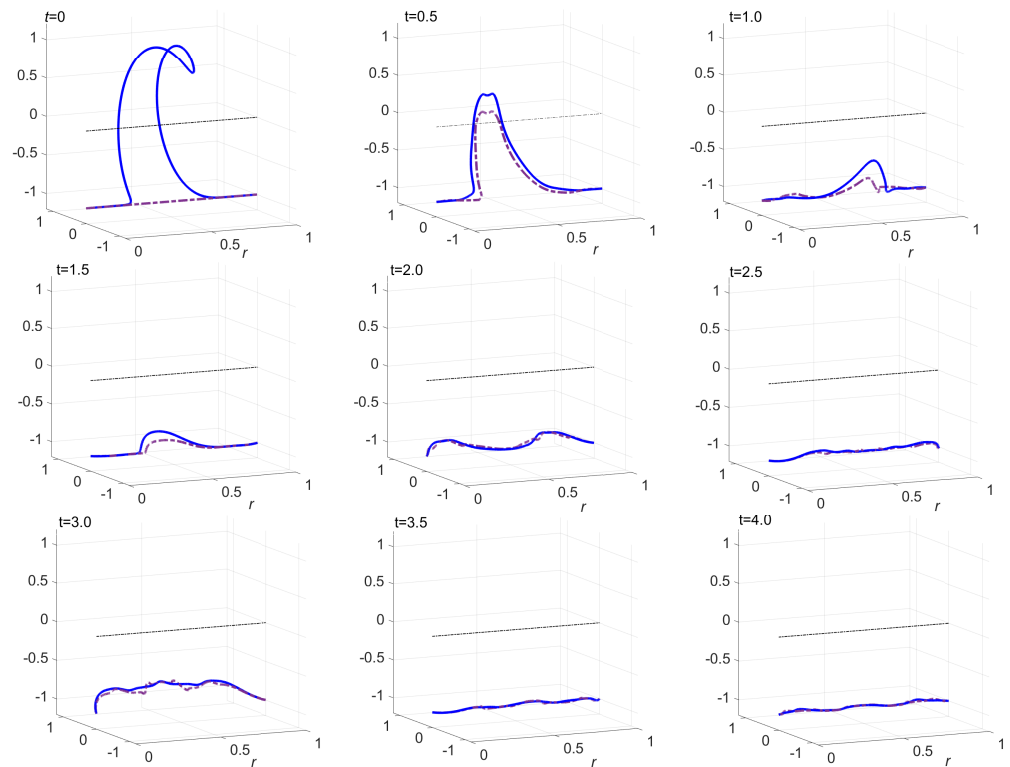


Figure 7. Feedback energy control (6), (18), ideal channel. The time histories of  $x(r, t)$ ,  $\xi(r, t)$ , estimation error  $x(r, t) - \xi(r, t)$  for  $r = 0.5$  (left plot), and  $r = 0.75$  (right plot).

By the analogy with Figure 4, a visual representation of the system behavior and the state estimation process is demonstrated in Figure 8 for instants  $t_i = 0, 0.5, 1.0 \dots, 4.0$ .



**Figure 8.** State estimation. Energy control (6), (18), ideal channel. The visual representation of the system behavior and its state estimation process.

### 5.3. Free Motion–State Estimation over Limited Capacity Communication Channel

#### 5.3.1. Free Motion State Estimation, First-Order Coder

##### Time-Invariant Coding

The first-order time-invariant coder/decoder pair is governed by (28), (29), (34), (35). For the simulations, the control signal  $u(r, t)$  was set to zero,  $u(r, t) \equiv 0$ , that produces free oscillations of the sine-Gordon chain (1), (2). Parameters of (33) were taken as  $\alpha = 1.05$ ,  $L_y = 15$  for each of  $l = 5$  sensors.

For each simulation runs, the following transmission rates were set (equal for every channel):

$$R = 1/T_s \in [10, 50, 100, 200, 400, 500, 1000], \text{ bit/s.} \tag{47}$$

The time histories of  $V(t)$  for various  $R$  (logarithmically scaled), along with the spatiotemporal plot of  $u_{\text{obs}}(r, t)$  (see (46)), calculated for  $R = 400$  bit/s,  $t \in [0.10]$  s, are depicted in Figure 9.

Taking into account that  $V(0) = 82.1$ , the following values of the quality indices are found:

$$V(t_{\text{fin}}) = [0.0501 \quad 0.0534 \quad 0.0571 \quad 0.1038 \quad 0.5645 \quad 3.221 \quad 106.2]$$

$$t_{\text{tr}}^V = [5.340 \quad 5.335 \quad 5.330 \quad 5.320 \quad \infty \quad \infty \quad \infty]$$

It is clear that although  $V(t)$  for  $R = 100$  bit/s falls in the given threshold, it tends to increase. Therefore, the case of  $R = 100$  bit/s should also be regarded as the state estimation failure. The conclusion can be made that for  $R \geq 200$  bit/s and given initial conditions (44), observer (26), (27) with the quantized measurements signals, produces the admissibly accurate state estimate for free motion of the sine-Gordon chain (1), (2). The transient time  $t_{\text{tr}}$  of the estimation is approximately 5.3 s, which is practically the same as for the ideal case of Section 5.2.1.

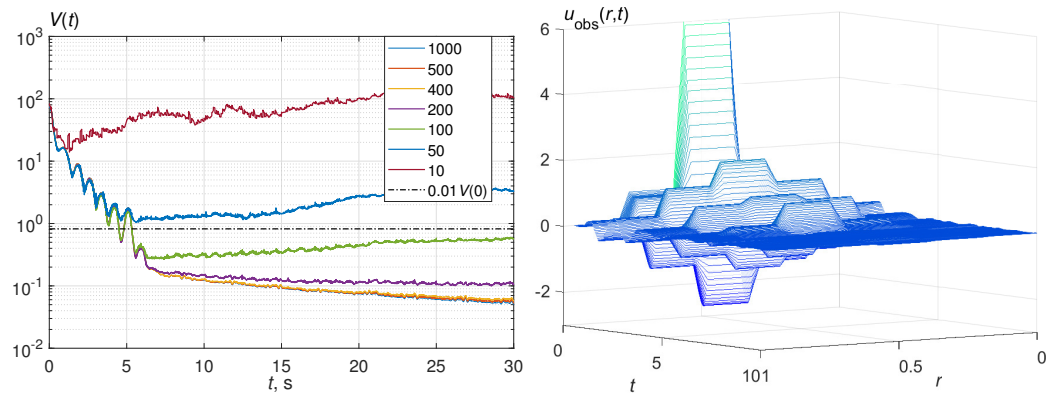


**Figure 9.** State estimation. Free motion case,  $u(r, t) \equiv 0$ . First-order time-invariant coder (28), (29).  $V(t)$  time histories for  $R$  as in (47) (left plot);  $u_{\text{obs}}(r, t)$  spatiotemporal plot for  $R = 400$  bit/s (right plot).

**Adaptive Coding**

The adaptive coding procedure for the first-order coder/decoder pair is described by (28), (29), (34), (35), where the quantization range  $M[k]$  is recursively found on the coder, and, synchronously, on the decoder side by (43). As above,  $u(r, t) \equiv 0, \alpha = 1.05$  were taken;  $L_y = 0.5$  was set for all five channels. Parameter  $\rho$  in (43) was calculated for an every single  $R$  as

$$\rho = \exp(-\eta T_s), \tag{48}$$

where  $\eta > 0$  is a design parameter. Such a parameter setting leads to the same rate of change  $M(t_k)$  in real (continuous) time independently of the sampling interval  $T_s = 1/R$ . In what follows,  $\eta = 0.6$  is taken.

The simulations were performed for the values of  $R$ , given by (47). The results are demonstrated in Figure 10, where for various  $R$ , the time histories of logarithmically scaled  $V(t)$  along with the plots of adaptively tunes quantizer range  $M_{0.5}(t)$  around the point  $r = 0.5$  are depicted. It is seen from the simulation results that for all considered values of  $R$ , save  $R = 10$  bit/s, the state estimation procedure convergences on time.

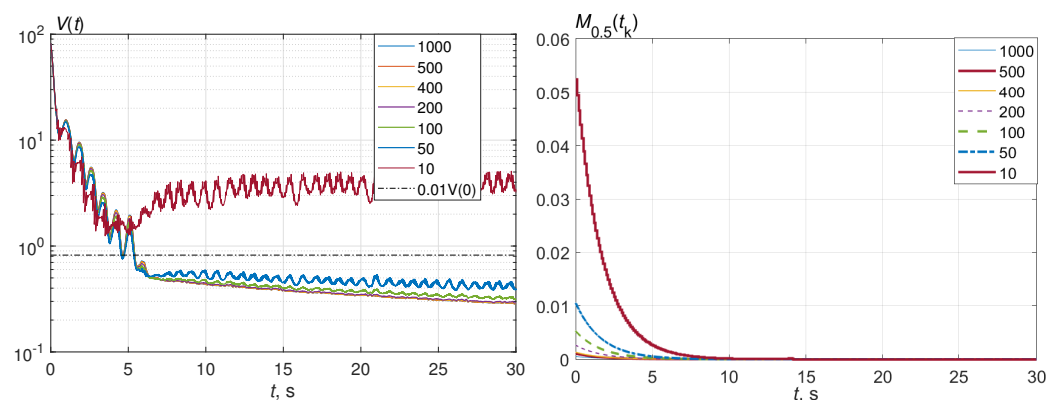


**Figure 10.** State estimation. Free motion case,  $u(r, t) \equiv 0$ . First-order adaptive coder (28), (29), (43).  $V(t)$  time histories for  $R$  as in (47) (left plot);  $M_{0.5}(t)$  time histories for  $r = 0.5$  (right plot).

Since  $V(0) = 82.1$ , the quality indices are as follows:

$$V(t_{\text{fin}}) = [0.285 \ 0.286 \ 0.286 \ 0.290 \ 0.314 \ 0.384 \ 3.207]$$

$$t_{\text{tr}}^V = [5.425 \ 5.425 \ 5.420 \ 5.410 \ 5.395 \ 5.375 \ \infty]$$

Compared with the time-invariant coder of the previous subsection, it is seen that the transmission rate range is wider, and the lowest admissible rate (among the considered ones, given in (47)) is 50 bit/s for each channel. This effect is because the adaptive encoder automatically reduces the quantization level when the behavior of the process allows it. In addition, in each section  $[r_j, r_{j+1}]$ ,  $j = 1, \dots, l - 1$ , the forms of  $x(r_j, t)$  oscillations in time for the sine-Gordon system are different, and their time derivatives slow down nearby the boundaries (where are zero). This peculiarity is automatically tracked by adaptive coding, ensuring the different  $M_j(t_k)$  for various sensors. It is also worth mentioning that, for the free motion state estimation, the transient time for considered above data transmission schemes is approximately the same for all considered above cases (and is about 5.3–5.5 s).

### 5.3.2. Free Motion State Estimation, Coder of Full Order

Let us examine the time-invariant and adaptive coding procedures for the full-order coder/decoder pair in the case of uncontrolled (free) motion of the chain.

The full-order encoder procedure assumes the inclusion of state observers in both the coder and decoder algorithms, and the observer on the decoder side generates the required plant state estimates. For the system under consideration, the coder-side observer is described by Equations (36), (37), when the observer on the decoder-side is described by (41), (42). The coder-generated update signals  $\bar{\varepsilon}_j$ ,  $j = 1, \dots, 5$ , are transmitted through the communication channel to correct the estimation process in the decoder-side observer.

#### Time-Invariant Coding

The time-invariant coding procedure uses (38)–(40) for  $\varepsilon_j(t)$  quantization and transmission to the receiver.

The simulations were performed for the values of  $R$ , given by (47),  $L_y = 0.5$ . The results are demonstrated in Figure 11, where for various  $R$ , the time histories of logarithmically scaled  $V(t)$  and the spatiotemporal plot of  $u_{\text{obs}}(r, t)$  (see (46)), calculated for  $R = 400$  bit/s,  $t \in [0, 10]$  s, are depicted.

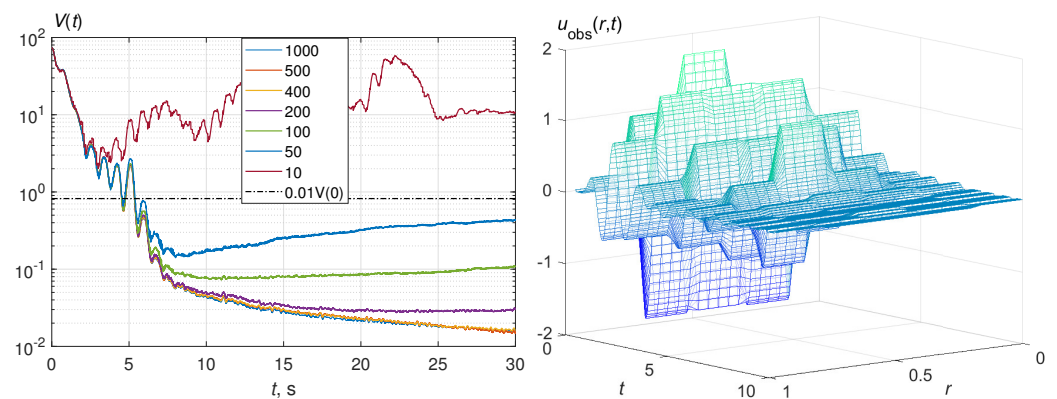


**Figure 11.** State estimation. Free motion case,  $u(r, t) \equiv 0$ . Full-order time-invariant coder (36), (37), observer on the decoder-side (41), (42).  $V(t)$  time histories for  $R$  as in (47) (left plot);  $u_{\text{obs}}(r, t)$  spatiotemporal plot for  $R = 400$  bit/s (right plot).

The simulations give the following quality indices:

$$V(t_{\text{fin}}) = [0.0151 \quad 0.0148 \quad 0.0160 \quad 0.0303 \quad 0.109 \quad 0.443 \quad 10.6]$$

$$t_{\text{tr}}^V = [ \quad 5.382 \quad 5.367 \quad 5.357 \quad 5.352 \quad \infty \quad \infty \quad \infty ]$$

Again, despite  $V(t)$  for  $R = 50$  and  $R = 100$  bit/s falling into the threshold value as  $0.01V(0)$ , these cases are also reasonable to refer to as unacceptable ones since  $V(t)$  increases after a certain time interval of fading. Therefore, the case of  $R = 200$  bit/s for each channel can be considered as a boundary one for this type of coder. Compared with the case of time-invariant first-order coding, one can notice that the values of  $V(t_{\text{fin}})$  are

significantly less than those for first-order coding, which shows better accuracy of the state estimation by the full-order coder. The same conclusion can also be made compared with the corresponding results for adaptive first-order coding. Regarding the transient time, the conclusion can be made that it also falls within the mentioned interval 5.3 s–5.5 s.

### Adaptive Coding

Consider now the application of the adaptive coding procedure (38)–(40), (43) with a full-order coder/decoder pair (36)–(41) for estimating the system state in free motion. For the simulation, the following values are taken  $\alpha = 1.05$ ,  $L_y = 0.5$  for all five channels; parameter  $\rho$  was calculated by (48), where  $\eta = 0.6$  was set.

The simulations were performed for the values of  $R$ , given by (47). The results are demonstrated in Figure 12, where for various  $R$ , time histories of logarithmically scaled  $V(t)$  along with the plots of adaptively tunes quantizer range  $M_{0.5}(t)$ , also logarithmically scaled, around the point  $r = 0.5$ , are depicted. It is seen from the simulation results that for all considered values of  $R$  starting from  $R = 50$  bit/s, the state estimation procedure converges on time, and after a short period of increasing,  $M_{0.5}(t)$  gradually decreases. This corresponds to increasing the estimation accuracy on time.

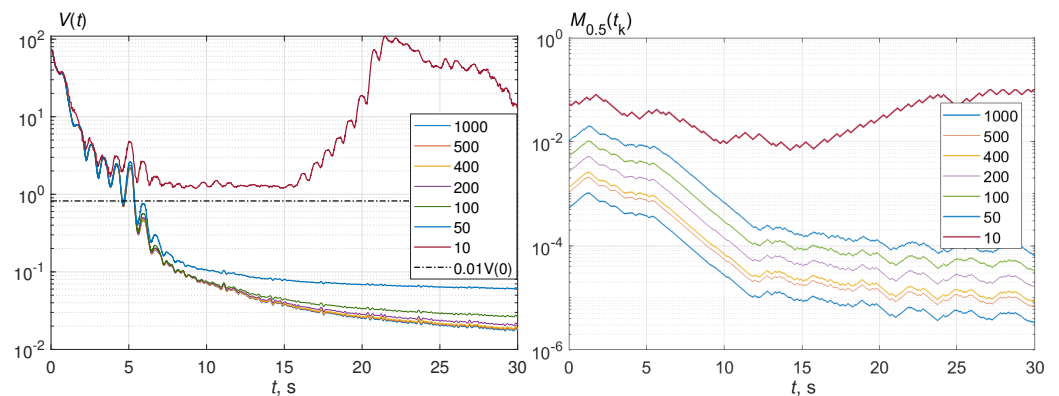


**Figure 12.** State estimation. Free motion case,  $u(r, t) \equiv 0$ . Full-order adaptive coder (38)–(40), (43).  $V(t)$  time histories for  $R$  as in (47) (left plot);  $M_{0.5}(t)$  time histories for  $r = 0.5$  (right plot).

The simulations give the following quality indices:

$$V(t_{fin}) = [0.0173 \quad 0.0178 \quad 0.0183 \quad 0.0203 \quad 0.0261 \quad 0.0602 \quad 12.29]$$

$$t_{tr}^V = [5.357 \quad 5.358 \quad 5.359 \quad 5.362 \quad 5.367 \quad 5.378 \quad \infty]$$

As can be seen from the data obtained, the convergence of the estimates is achieved at a data bitrate of 50 bits per second and is kept as  $R$  increases. The decay time of the estimation error lies in the range 5.3–5.5 s, as well as above, but this encoding method leads to significantly smaller estimation errors. In comparison with adaptive first-order coding, however, the question arises: does the complication of the estimation procedure and the associated computational costs pay off the increase in the estimation accuracy? The answer to this question requires further research and can hardly be given outside the framework of solving a specific physical or technical problem.

### 5.4. Output Control of Energy–State Estimation over Limited Capacity Communication Channel

In this subsection, the closed-loop energy control problem via output feedback is examined. The closed-loop energy control system is described by (1), (2), (24), (25), where the controller, instead of  $x(r, t)$ ,  $x_t(r, t)$ , used by the ideal state-feedback energy control law (6), (18), employs the state estimates  $\zeta(r, t)$ ,  $\zeta_t(r, t)$  obtained by the state observer where measured data in the observer input are transferred over the limited capacity communication channel. Control action  $u(r, t)$  is assumed to be accurately known to the observer. For the given initial conditions (44) and  $E_* = 5$ , it is valid that  $\Delta E(0) = -15.7$ ,  $V(0) = 82.1$ .

Note that an ideal energy control case is numerically studied in Section 5.2.2, where the state feedback control law (18) is used.

### 5.4.1. Output Control of Energy, First-Order Coder Time-Invariant Coding

In this paragraph, the case of output feedback energy control with the time-invariant first-order coder is studied. The coder/decoder pair, governed by (28), (29), (34), (35) is employed. Parameters of (33) were taken as  $\alpha = 1.05$ ,  $L_y = 15$  for each of  $l = 5$  sensors. The control law (24), (25) uses the estimates  $\zeta, \zeta$  generated by observer (22), (23). As in Section 5.2.2, the controller gains  $\gamma_i$  are taken as  $\gamma_i = 22.8$  for  $i = 1, \dots, 10$ , and the desired energy level  $E_* = 5$  was set.

Time histories of  $E(t), V(t)$  are plotted in Figure 13 for various values of  $R$  from (47).

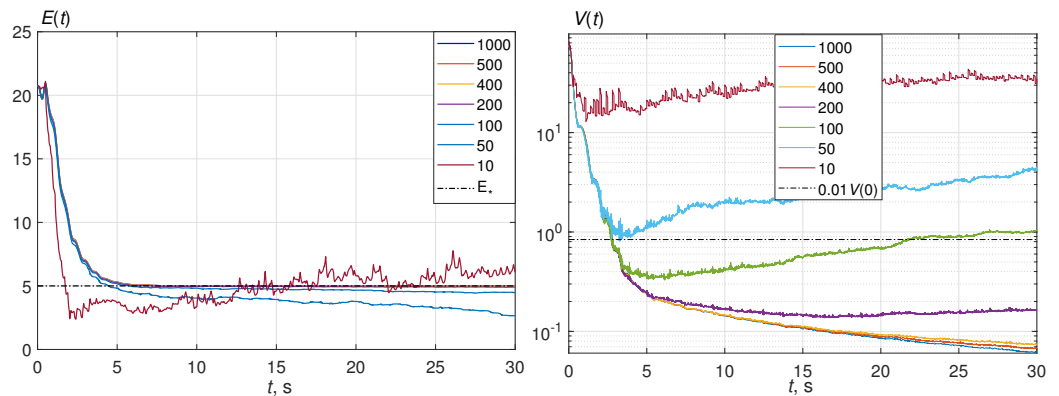


**Figure 13.** Output control law (22)–(25). First-order time-invariant coder (28), (29). Time histories of  $E(t)$  (left plot),  $V(t)$  (right plot).

The simulations give the following quality indices:

$$\begin{aligned}
 V(t_{\text{fin}}) &= [0.0618 \quad 0.0675 \quad 0.0737 \quad 0.166 \quad 1.035 \quad 4.501 \quad 34.87] \\
 \Delta E(t_{\text{fin}}) &= [0.009 \quad 0.014 \quad 0.027 \quad 0.097 \quad 0.502 \quad 2.320 \quad -1.450] \\
 t_{\text{tr}}^V &= [2.755 \quad 2.78 \quad 2.79 \quad 2.80 \quad \infty \quad \infty \quad \infty] \\
 t_{\text{tr}}^E &= [5.157 \quad 5.615 \quad 5.133 \quad 5.163 \quad \infty \quad \infty \quad \infty]
 \end{aligned}$$

As is seen from the results obtained, the minimal appropriate data transmission rate is 200 bit/s for each channel. The state estimation transient time  $t_{\text{tr}}^V$  lies between 2.7 s–2.8 s, while the energy control transient time  $t_{\text{tr}}^E$  is between 5.2 s–5.7 s for all suitable data transmission rates.

### Adaptive Coding

In this series of simulations, the output feedback energy control with the adaptive first-order coder is studied. The coder/decoder pair is governed by (28), (29), (34), (35), (43), where for (33),  $\alpha = 1.05$ ,  $L_y = 0.5$  were set to all sensors. The control law (24), (25) uses the estimates  $\zeta, \zeta$  generated by observer (22), (23). As in Section 5.2.2, the controller gains  $\gamma_i$  are taken as  $\gamma_i = 22.8$ , and  $E_* = 5$  was set.

Time histories of  $E(t), V(t)$  are plotted in Figure 14 for various values of  $R$  from (47). The simulations give the following quality indices:

$$\begin{aligned}
 V(t_{\text{fin}}) &= [0.295 \quad 0.295 \quad 0.295 \quad 0.296 \quad 0.302 \quad 0.328 \quad 2.812] \\
 \Delta E(t_{\text{fin}}) &= [0.0780 \quad 0.0785 \quad 0.0902 \quad 0.1038 \quad 0.1044 \quad 0.1052 \quad 0.860] \\
 t_{\text{tr}}^V &= [3.445 \quad 3.440 \quad 3.435 \quad 3.395 \quad 3.360 \quad 3.315 \quad \infty] \\
 t_{\text{tr}}^E &= [5.815 \quad 5.835 \quad 5.790 \quad 5.720 \quad 5.700 \quad 5.680 \quad \infty]
 \end{aligned}$$

It is seen from the results, the data transmission rate can be taken as low as 50 bit/s, the observer transient time  $t_{tr}^V$  lies between 3.34 s–3.36 s, while the energy control transient time  $t_{tr}^E$  is between 5.6 s–5.9 s for all data transmission rates except  $R = 10$  bit/s, where the considered output control procedure fails.

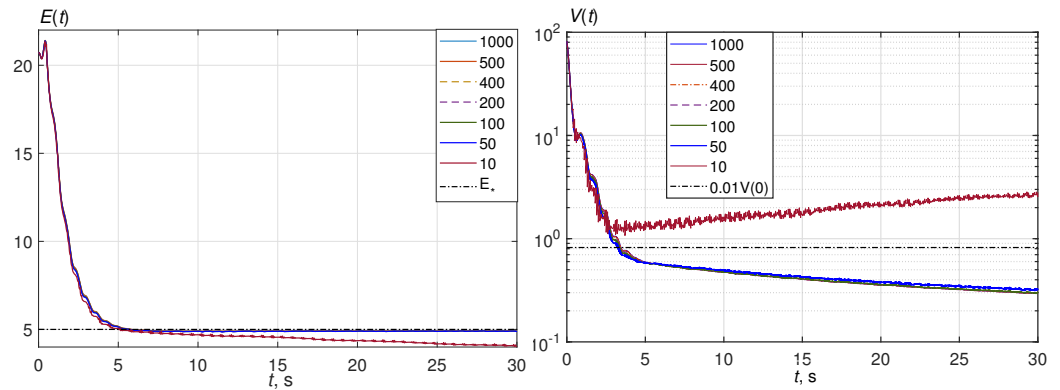


Figure 14. Output control law (22)–(25). First-order adaptive coder (28), (29), (43). Time histories of  $E(t)$  (left plot),  $V(t)$  (right plot).

#### 5.4.2. Output Control of Energy, Coder of Full Order Time-Invariant Coding

Let us examine the properties of the output feedback energy control system with the time-invariant coder of full order. The time-invariant coding procedure (38)–(40) is used for  $\varepsilon_j(t)$  quantization and transmission to the receiver. Transmission rate  $R$  for the simulations was taken from (47);  $\alpha = 1.05$ ,  $L_y = 0.5$ . The control law (22)–(25) uses the estimates  $\xi$ ,  $\zeta$  generated by the data transmission and state estimation procedure (38)–(40). The controller gains  $\gamma_i$  are taken as  $\gamma_i = 22.8$ , and  $E_* = 5$  was set.

The time histories of  $E(t)$ ,  $V(t)$  are plotted in Figure 15.

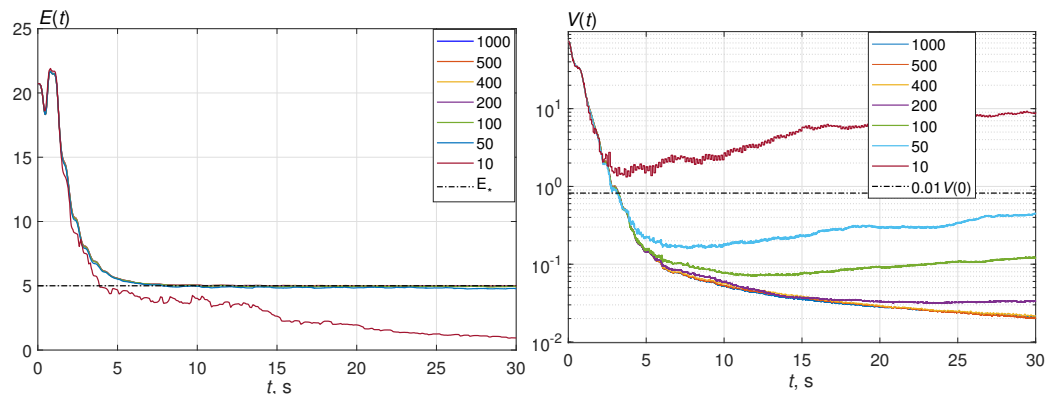


Figure 15. Output control law (22)–(25). Time-invariant coding procedure (38)–(40). Time histories of  $E(t)$  (left plot),  $V(t)$  (right plot).

The quality indices, calculated by the simulation results, are as follows:

$$\begin{aligned}
 V(t_{fin}) &= [0.0210 \quad 0.0202 \quad 0.0220 \quad 0.0338 \quad 0.1225 \quad 0.4551 \quad 8.9404] \\
 \Delta E(t_{fin}) &= [0.002 \quad 0.011 \quad 0.019 \quad 0.0302 \quad 0.075 \quad 0.232 \quad 4.060] \\
 t_{tr}^V &= [3.155 \quad 3.190 \quad 3.215 \quad 3.225 \quad \infty \quad \infty \quad \infty] \\
 t_{tr}^E &= [6.538 \quad 6.550 \quad 6.555 \quad 6.570 \quad \infty \quad \infty \quad \infty]
 \end{aligned}$$

Since for  $R = 100$  bit/s,  $V(t)$  increases after a certain decreasing interval; this case is also referred to as an inappropriate one.

### Adaptive Coding

Finally, consider the output feedback energy control system with the adaptive coder of full order. This coding procedure for quantization of  $\varepsilon_j(t)$  and transmission it the receiver is described by (38)–(40), (43). Transmission rate  $R$  for the simulations was taken from (47);  $\alpha = 1.05, L_y = 0.5$ . The control law (22)–(25) uses the estimates  $\xi, \zeta$  generated by the data transmission ans state estimation procedure (38)–(40). The controller gains  $\gamma_i$  are taken as  $\gamma_i = 22.8; E_* = 5$  was set.

The time histories of  $E(t), V(t)$  are plotted in Figure 16.

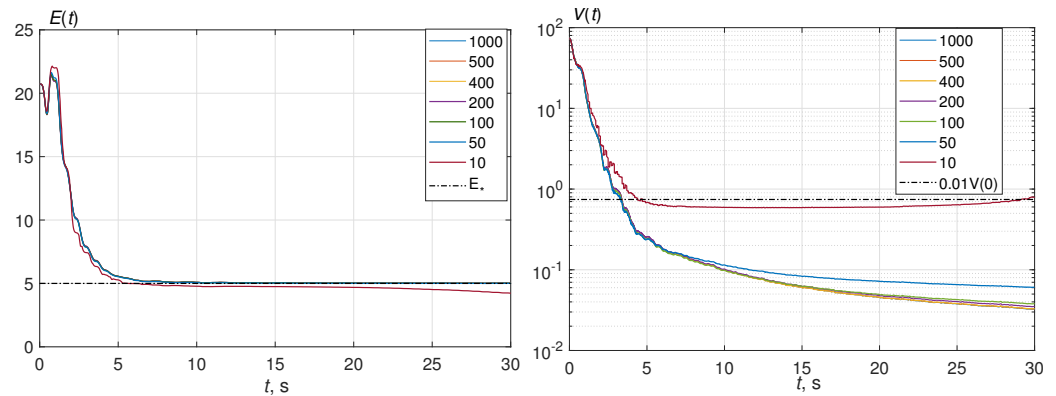


**Figure 16.** Output control law (22)–(25). Adaptive coding (38)–(40), (43). Time histories of  $E(t)$  (left plot),  $V(t)$  (right plot).

Based on the simulation results, the following quality indices are found:

$$\begin{aligned}
 V(t_{\text{fin}}) &= [0.0324 \quad 0.0327 \quad 0.0328 \quad 0.0350 \quad 0.0379 \quad 0.0606 \quad 0.7979] \\
 \Delta E(t_{\text{fin}}) &= [-0.0144 \quad -0.0143 \quad -0.0140 \quad -0.0139 \quad -0.0101 \quad 0.0017 \quad 0.753] \\
 t_{\text{tr}}^V &= [3.385 \quad 3.38 \quad 3.385 \quad 3.375 \quad 3.355 \quad 3.315 \quad \infty] \\
 t_{\text{tr}}^E &= [7.745 \quad 7.740 \quad 7.735 \quad 7.730 \quad 7.72 \quad 6.50 \quad \infty]
 \end{aligned}$$

It is seen from the results the minimal appropriate data transmission rate is as 50 bit/s, the observer transient time  $t_{\text{tr}}^V$  lies between 3.2 s–3.9 s, while the energy control transient time  $t_{\text{tr}}^E$  is between 6.5 s–7.5 s for all appropriate data transmission rates. The energy control static (final) error is less than all of the above in magnitude.

### 5.5. Consolidated Results

This section presents the combined results of the above performance scores for state estimation under free motion and simultaneous energy control with state estimation from the output. These results are summarized in Table 1 (estimation of state in free motion case) and Table 2 (control over state estimates). Combinations are highlighted in gray, in which data transmission over a digital channel with coding is not acceptable. As can be seen from the results, the best values of quality indicators are obtained with adaptive coding with a full-order coder/decoder pair. In this context, the question arises: does the complication of the estimation procedure and the associated computational costs pay off the increase in the estimation accuracy? In the Authors’ opinion, the answer to this question requires further research and can hardly be given outside the framework of solving a specific physical or technical problem.

**Table 1.** Free Motion State Estimation.

Section; Equation; Figure	Q. Fun.	Transmission Rate, bit/s						
		1000	500	400	200	100	50	10
Section 5.3.1		First-order Time-invariant Coder						
Equations (26)–(29) (34), (35); $u(r, t) \equiv 0$ ; Figure 9	$V(t_{\text{fin}})$	0.0501	0.0534	0.0571	0.104	0.564	3.22	106
	$t_{\text{tr}}^V$	5.340	5.335	5.330	5.320	$\infty$	$\infty$	$\infty$
Section 5.3.1		First-order Adaptive Coder						
Equations (26)–(29), (34) (35), (43); $u(r, t) \equiv 0$ ; Figure 10	$V(t_{\text{fin}})$	0.285	0.286	0.286	0.290	0.314	0.384	3.207
	$t_{\text{tr}}^V$	5.425	5.425	5.420	5.410	5.395	5.375	$\infty$
Section 5.3.2		Full-order Time-invariant Coder						
Equations (36)–(42), (34) (35); $u(r, t) \equiv 0$ ; Figure 11	$V(t_{\text{fin}})$	0.0151	0.0148	0.0160	0.0303	0.109	0.443	10.6
	$t_{\text{tr}}^V$	5.382	5.367	5.357	5.352	5.351	5.350	$\infty$
Section 5.3.2		Full-order Adaptive Coder						
Equations (36)–(42), (34) (35), (43); $u(r, t) \equiv 0$ ; Figure 12	$V(t_{\text{fin}})$	0.0173	0.0178	0.0183	0.0203	0.0261	0.0602	12.29
	$t_{\text{tr}}^V$	5.357	5.358	5.359	5.362	5.367	5.378	$\infty$

Note: the gray color background uses to stress the unfeasible cases.

**Table 2.** Output Control of Energy.

Section; Equation Figure	Q. Fun.	Transmission Rate, bit/s							
		1000	500	400	200	100	50	10	
Section 5.4.1		First-order Time-invariant Coder							
Equations (26)–(29) (34), (35) Figure 13	$V(t_{\text{fin}})$	0.0618	0.0675	0.0737	0.166	1.035	4.501	34.9	
	$t_{\text{tr}}^V$	2.755	2.78	2.79	2.80	$\infty$	$\infty$	$\infty$	
	$\Delta E(t_{\text{fin}})$	0.009	0.014	0.027	0.097	0.502	2.32	−1.450	
Section 5.4.1	Figure 14	$t_{\text{tr}}^E$	5.157	5.615	5.133	5.163	$\infty$	$\infty$	$\infty$
		First-order Adaptive Coder							
		$V(t_{\text{fin}})$	0.295	0.295	0.295	0.296	0.302	0.328	2.812
Equations (26)–(29) (34), (35), (43) Figure 14	$t_{\text{tr}}^V$	3.44	3.44	3.43	3.39	3.36	3.31	$\infty$	
	$\Delta E(t_{\text{fin}})$	0.078	0.078	0.090	0.104	0.104	0.105	0.86	
	$t_{\text{tr}}^E$	5.815	5.835	5.790	5.720	5.700	5.680	$\infty$	
Section 5.4.2		Full-order Time-invariant Coder							
Equations (36)–(42) (34), (35) Figure 15	$V(t_{\text{fin}})$	0.0210	0.0202	0.0220	0.0338	0.1225	0.4551	8.940	
	$t_{\text{tr}}^V$	3.155	3.190	3.215	3.225	$\infty$	$\infty$	$\infty$	
	$\Delta E(t_{\text{fin}})$	0.002	0.011	0.019	0.0302	0.075	0.232	4.06	
Section 5.4.2	Figure 16	$t_{\text{tr}}^E$	6.538	6.550	6.555	6.570	$\infty$	$\infty$	$\infty$
		Full-order Adaptive Coder							
		$V(t_{\text{fin}})$	0.0324	0.0327	0.0328	0.0350	0.0379	0.0606	0.798
Equations (36)–(42) (34), (35), (43) Figure 16	$t_{\text{tr}}^V$	3.38	3.38	3.38	3.37	3.35	3.31	$\infty$	
	$\Delta E(t_{\text{fin}})$	0.0144	0.0143	0.0140	0.0139	0.0101	−0.002	−0.75	
	$t_{\text{tr}}^E$	7.745	7.740	7.735	7.730	7.72	6.50	$\infty$	

Note: the gray color background uses to stress the unfeasible cases.

## 6. Conclusions

This paper considers and studies the problem of controlling the energy of a nonlinear spatially distributed sine-Gordon system when transmitting measurements and estimating the state of the chain through digital communication channels of limited bandwidth. As part of the research, observation schemes with data transmission over a communication channel based on stationary and adaptive encoders of the first order, as well as full orders, are presented. The procedures for estimating the state during the free movement of the chain, as well as the control of its energy by output during data transmission over a digital information channel, are considered separately. Based on the results of numerical analysis, comparative applications of the characteristics of various coding schemes are obtained. It is shown that from the point of view of minimizing the channel load, estimation accuracy, and energy control, the adaptive first-order encoder has an advantage, but its use implies high computation costs, which may be unacceptable in specific technical applications. The present numerical study has confirmed the fundamental limitations of the underlying closed-loop nonlinear PDE to be locally asymptotically stable only. Establishing the domain of the initial states, which converge to the closed-loop equilibrium, calls for further numerical investigation and to be tackled along the line of the proposed development, hopefully. Studies of the possibility of using encoders of “intermediate” (finite) orders, as well as the effects of measurement noise and in the communication channel, are planned for investigations in the future.

**Author Contributions:** Conceptualization, B.A. and A.L.F.; data curation, B.A. and Y.O.; formal analysis, Y.O. and A.L.F.; funding acquisition, A.L.F.; investigation, B.A.; methodology, B.A. and Y.O.; project administration, A.L.F.; software, B.A.; supervision, Y.O. and A.L.F.; writing—original draft, B.A.; writing—review & editing, all authors. All authors have read and agreed to the published version of the manuscript.

**Funding:** This work was supported by the Ministry of Science and Higher Education of the Russian Federation (Project No. 075-15-2021-573, performed in the IPME RAS).

**Data Availability Statement:** Not applicable.

**Conflicts of Interest:** The authors declare no conflict of interest.

## Abbreviations

The following abbreviations and notations are used in this manuscript:

1-D	One-Dimensional
BVP	Boundary-Value Problem
LMI	Linear Matrix Inequality
MEMS	Microelectromechanical Systems
ODE	Ordinary Differential Equation
PDE	Partial Differential Equation
SG	Speed-Gradient
$L_2$	$L_2$ -norm of a vector $x$ is $\ x\ ^2$
$H^1(a, b)$	Sobolev space
$\text{supp}(f)$	Support of function $f : \mathbb{R}^k \rightarrow \mathbb{R}$ —the smallest closed set containing all the points $x \in \mathbb{R}^k$ where $f(x) \neq 0$
$\mathbb{Z}$	set of nonnegative integer numbers, $\mathbb{Z} = \{0, 1, \dots\}$
$x_t$	$x_t \equiv \frac{\partial x}{\partial t}$
$x_{tt}$	$x_{tt} \equiv \frac{\partial^2 x}{\partial t^2}$
$x_r'$	$x_r' \equiv \frac{\partial x}{\partial r}$
$x_{rt}$	$x_{rt} \equiv \frac{\partial^2 x}{\partial r \partial t}$
$x''$	$x'' \equiv \frac{\partial^2 x}{\partial r^2}$

## References

1. Siang, J.; Lim, M.H.; Leong, M.S. Review of vibration-based energy harvesting technology: Mechanism and architectural approach. *Intern. J. Energy Res.* **2018**, *42*, 1866–1893. [[CrossRef](#)]
2. Leong, A.S.; Dey, S.; Quevedo, D.E. Transmission scheduling for remote state estimation and control with an energy harvesting sensor. *Automatica* **2018**, *91*, 54–60. [[CrossRef](#)]
3. Nikpoorparizi, P.; Deodhar, N.; Vermillion, C. Modeling, Control Design, and Combined Plant/Controller Optimization for an Energy-Harvesting Tethered Wing. *IEEE Trans. Control Syst. Technol.* **2018**, *26*, 1157–1169. [[CrossRef](#)]
4. Boussaid, N.; Caponigro, M.; Chambrion, T. Total Variation of the Control and Energy of Bilinear Quantum Systems. In Proceedings of the 52nd IEEE Conference on Decision and Control (CDC 2013), Firenze, Italy, 10–13 December 2013; pp. 3714–3719.
5. Bonnard, B.; Caillaud, J.B.; Cots, O. Energy Minimization In Two-Level Dissipative Quantum Control: The Integrable Case. *Discret. Contin. Dyn. Syst.* **2011**, *31*, 198–208.
6. Mantile, A. Point interaction controls for the energy transfer in 3-D quantum systems. *Intern. J. Control* **2008**, *81*, 752–763. [[CrossRef](#)]
7. Andrievsky, B.; Fradkov, A.L. Speed Gradient Method and Its Applications. *Autom. Remote Control* **2021**, *82*, 1463–1518. [[CrossRef](#)]
8. Orlov, Y.; Fradkov, A.L.; Andrievsky, B. Output Feedback Energy Control of the sine-Gordon PDE Model Using Collocated Spatially Sampled Sensing and Actuation. *IEEE Trans. Autom. Control* **2020**, *65*, 1484–1498. [[CrossRef](#)]
9. Fridman, E. A refined input delay approach to sampled-data control. *Automatica* **2010**, *46*, 421–427. [[CrossRef](#)]
10. Fridman, E.; Seuret, A.; Richard, J.P. Robust sampled-data stabilization of linear systems: An input delay approach. *Automatica* **2004**, *40*, 1441–1446. [[CrossRef](#)]
11. Balas, M.J. Toward a more practical control theory for distributed parameter systems. In *Advances in Theory and Applications*; Leondes, C., Ed.; Academic Press: Cambridge, MA, USA, 1982; Volume 18, pp. 361–421.
12. Curtain, R.; Zwart, H. An Introduction to Infinite-Dimensional Linear Systems Theory. In *Texts in Applied Mathematics*; Springer: Heilderberg, Germany, 1995; Volume 21.
13. Koga, S.; Karafyllis, I.; Krstic, M. Towards implementation of PDE control for Stefan system: Input-to-state stability and sampled-data design. *Automatica* **2021**, *127*, 109538. [[CrossRef](#)]
14. Wang, J.W. Exponentially Stabilizing Observer-Based Feedback Control of a Sampled-Data Linear Parabolic Multiple-Input–Multiple-Output PDE. *IEEE Trans. Syst. Man Cybern.* **2021**, *51*, 5742–5751. [[CrossRef](#)]
15. Katz, R.; Fridman, E. Sampled-data finite-dimensional boundary control of 1D parabolic PDEs under point measurement via a novel ISS Halanay’s inequality. *Automatica* **2022**, *135*, 109966. [[CrossRef](#)]
16. Ahmed-Ali, T.; Karafyllis, I.; Giri, F. Sampled-data observers for delay systems and hyperbolic PDE–ODE loops. *Automatica* **2021**, *123*, 109349. [[CrossRef](#)]
17. Andrievsky, B.; Orlov, Y.; Fradkov, A. On robustness of the speed-gradient sampled-data energy control for the sine–Gordon equation: The simpler the better. *Commun. Nonlinear Sci. Numer. Simul.* **2023**, *117*, 106901. [[CrossRef](#)]
18. Cuevas-Maraver, J.; Kevrekidis, P.; Williams, F. (Eds.) *The Sine-Gordon Model and Its Applications. From Pendula and Josephson Junctions to Gravity and High-Energy Physics*; Springer: Cham, Switzerland, 2014.
19. Kobayashi, T. Boundary feedback stabilization of the sine-Gordon equation without velocity feedback. *J. Sound Vib.* **2003**, *266*, 775–784. [[CrossRef](#)]
20. Petcu, M.; Temam, R. Control for the sine-Gordon equation. *ESAIM Control Optim. Calc. Var.* **2004**, *10*, 553–573. [[CrossRef](#)]
21. Kobayashi, T. Adaptive stabilization of the sine-Gordon equation by boundary control. *Math. Methods Appl. Sci.* **2004**, *27*, 957–970. [[CrossRef](#)]
22. Hastir, A.; Winkin, J.J.; Dochain, D. Funnel control for a class of nonlinear infinite-dimensional systems. *Automatica* **2023**, *152*, 110964. [[CrossRef](#)]
23. Dmitriev, S.V.; Shigenari, T.; Abe, K.; Vasiliev, A.A.; Miroshnichenko, A.E. Phonon emission from a discrete sine-Gordon breather. *Comput. Mater. Sci.* **2000**, *18*, 303–307. [[CrossRef](#)]
24. Kivshar, Y.S.; Benner, H.; Braun, O.M. Nonlinear Models for the Dynamics of Topological Defects in Solids. In *Proceedings of the Nonlinear Science at the Dawn of the 21st Century*; Christiansen, P.L., Sørensen, M.P., Scott, A.C., Eds.; Springer: Berlin/Heidelberg, Germany, 2000; pp. 265–291.
25. Malomed, B.A. The sine-Gordon Model: General Background, Physical Motivations, Inverse Scattering, and Solitons. In *The Sine-Gordon Model and Its Applications: From Pendula and Josephson Junctions to Gravity and High-Energy Physics*; Cuevas-Maraver, J., Kevrekidis, P.G., Williams, F., Eds.; Springer International Publishing: Cham, Switzerland, 2014; pp. 1–30. [[CrossRef](#)]
26. Cen, J.; Correa, F.; Fring, A. Degenerate multi-solitons in the sine-Gordon equation. *J. Phys. A Math. Theor.* **2017**, *50*, 435201. [[CrossRef](#)]
27. Sickotra, S. Solitons: Kinks, Collisions and Breathers. *arXiv* **2021**, arXiv:2103.12916.
28. Zhou, Q.; Ekici, M.; Mirzazadeh, M.; Sonmezoglu, A. The investigation of soliton solutions of the coupled sine-Gordon equation in nonlinear optics. *J. Mod. Opt.* **2017**, *64*, 1677–1682. [[CrossRef](#)]
29. Gershenzon, N.I.; Bambakidis, G.; Skinner, T.E. Sine-Gordon modulation solutions: Application to macroscopic non-lubricant friction. *Phys. D Nonlinear Phenom.* **2016**, *333*, 285–292. [[CrossRef](#)]
30. Leung, K. Mechanical properties of double-sine-Gordon solitons and the application to anisotropic Heisenberg ferromagnetic chains. *Phys. Rev. B* **1983**, *27*, 2877–2888. [[CrossRef](#)]

31. Herbut, I. Dual theory of the superfluid-Bose-glass transition in the disordered Bose-Hubbard model in one and two dimensions. *Phys. Rev. B-Condens. Matter Mater. Phys.* **1998**, *57*, 13729–13742. [[CrossRef](#)]
32. Temam, R. *Infinite-Dimensional Dynamical Systems in Mechanics and Physics*; Applied mathematical sciences; Springer: New York, NY, USA, 1997.
33. Refael, G.; Demler, E.; Oreg, Y.; Fisher, D.S. Dissipation and quantum phase transitions of a pair of Josephson junctions. *Phys. Rev. B-Condens. Matter Mater. Phys.* **2003**, *68*, 214515. [[CrossRef](#)]
34. Cirillo, M.; Parmentier, R.; Savo, B. Mechanical analog studies of a perturbed sine-Gordon equation. *Phys. D Nonlinear Phenom.* **1981**, *3*, 565–576. [[CrossRef](#)]
35. Fradkov, A.; Andrievsky, B.; Boykov, K. Multipendulum mechatronic setup: Design and experiments. *Mechatronics* **2012**, *22*, 76–82. [[CrossRef](#)]
36. Do, L.; Hurák, Z. Synchronization in the Frenkel-Kontorova Model with Application to Control of Nanoscale Friction. *IFAC-PapersOnLine* **2021**, *54*, 406–411. [[CrossRef](#)]
37. Do, L.; Pučejdl, K.; Hurák, Z. Experimental Platform for Boundary Control of Mechanical Frenkel-Kontorova Model. In Proceedings of the 2022 IEEE 61st Conference on Decision and Control (CDC 2022), Cancun, Mexico, 6–9 December 2022; pp. 7618–7623. [[CrossRef](#)]
38. Athans, M. Toward a practical theory for distributed parameter systems. *IEEE Trans. Autom. Control* **1970**, *15*, 245–247. [[CrossRef](#)]
39. Nair, G.N.; Evans, R.J. State Estimation under Bit-Rate Constraints. In Proceedings of the 37th IEEE Conference on Decision and Control, Tampa, FL, USA, 16–18 December 1998; Volume WA09, pp. 251–256.
40. Elia, N.; Mitter, S.K. Stabilization of Linear Systems with Limited Information. *IEEE Trans. Autom. Control* **2001**, *46*, 1384–1400. [[CrossRef](#)]
41. Tatikonda, S.; Mitter, S. Control under communication constraints. *IEEE Trans. Autom. Control* **2004**, *49*, 1056–1068. [[CrossRef](#)]
42. Matveev, A.S.; Savkin, A.V. The Problem of State Estimation via Asynchronous Communication Channels with Irregular Transmission Times. *IEEE Trans. Autom. Control* **2003**, *48*, 670–676. [[CrossRef](#)]
43. Nair, G.N.; Evans, R.J. Stabilizability of stochastic linear systems with finite feedback data rates. *SIAM J. Control Optim* **2004**, *43*, 413–436. [[CrossRef](#)]
44. Nair, G.N.; Evans, R.J. Exponential stabilizability of finite-dimensional linear systems with limited data rates. *Automatica* **2003**, *39*, 585–593. [[CrossRef](#)]
45. Nair, G.N.; Fagnani, F.; Zampieri, S.; Evans, R. Feedback control under data rate constraints: An overview. *Proc. IEEE* **2007**, *95*, 108–137. [[CrossRef](#)]
46. Matveev, A.S.; Savkin, A.V. *Estimation and Control over Communication Networks*; Birkhäuser: Boston, MA, USA, 2009.
47. Aslmostafa, E.; Ghaemi, S.; Badamchizadeh, M.A.; Ghiasi, A.R. Adaptive backstepping quantized control for a class of unknown nonlinear systems. *ISA Trans.* **2022**, *125*, 146–155. [[CrossRef](#)]
48. Andrievsky, B.; Fradkov, A.L.; Peaucelle, D. Estimation and Control under Information Constraints for LAAS Helicopter Benchmark. *IEEE Trans. Control Syst. Technol.* **2010**, *15*, 1180–1187. [[CrossRef](#)]
49. De Persis, C. On stabilization of nonlinear systems under data rate constraints using output measurements. *Int. J. Robust Nonlinear Control* **2006**, *16*, 315–332. [[CrossRef](#)]
50. Cheng, T.M.; Savkin, A.V. Output feedback stabilisation of nonlinear networked control systems with non-decreasing nonlinearities: A matrix inequalities approach. *Int. J. Robust Nonlinear Control* **2007**, *17*, 387–404. [[CrossRef](#)]
51. Brockett, R.W.; Liberzon, D. Quantized Feedback Stabilization of Linear Systems. *IEEE Trans. Autom. Control* **2000**, *45*, 1279–1289. [[CrossRef](#)]
52. Liberzon, D. Hybrid feedback stabilization of systems with quantized signals. *Automatica* **2003**, *39*, 1543–1554. [[CrossRef](#)]
53. Moreno-Alvarado, R.; Rivera-Jaramillo, E.; Nakano, M.; Perez-Meana, H. Simultaneous Audio Encryption and Compression Using Compressive Sensing Techniques. *Electronics* **2020**, *9*, 863. [[CrossRef](#)]
54. Goodman, D.J.; Gersho, A. Theory of an Adaptive Quantizer. *IEEE Trans. Commun.* **1974**, COM-22, 1037–1045. [[CrossRef](#)]
55. Gomez-Estern, F.; Canudas de Wit, C.; Rubio, F. Adaptive delta modulation in networked controlled systems with bounded disturbances. *IEEE Trans. Autom. Control* **2011**, *56*, 129–134. [[CrossRef](#)]
56. Delchamps, D.F. Stabilizing a linear system with quantized state feedback. *IEEE Trans. Autom. Control* **1990**, *35*, 916–924. [[CrossRef](#)]
57. Baillieul, J. Feedback coding for information-based control: Operating near the data rate limit. In Proceedings of the 41st IEEE Conf. on Decision & Control, Las Vegas, NV, USA, 10–13 December 2002; Volume ThP02-6, pp. 3229–3236.
58. De Persis, C. A Note on Stabilization via Communication Channel in the presence of Input Constraints. In Proceedings of the 42nd IEEE Conference on Decision & Control, Maui, HI, USA, 9–12 December 2003; Volume TuA06-3, pp. 187–192.
59. De Persis, C. n-Bit Stabilization of n-Dimensional Nonlinear Systems in Feedforward Form. *IEEE Trans. Autom. Control* **2005**, *50*, 299–311. [[CrossRef](#)]
60. Fradkov, A.L.; Andrievsky, B.; Ananyevskiy, M.S. Passification based synchronization of nonlinear systems under communication constraints and bounded disturbances. *Automatica* **2015**, *55*, 287–293. [[CrossRef](#)]
61. Goodwin, G.; Lau, K.; Cea, M. Control with communication constraints. In Proceedings of the 12th Int. Conf. on Control Automation Robotics & Vision (ICARCV 2012), Guangzhou, China, 5–7 December 2012; pp. 1–10. [[CrossRef](#)]

62. Paranjape, A.; Guan, J.; Chung, S.J.; Krstic, M. PDE boundary control for flexible articulated wings on a robotic aircraft. *IEEE Trans. Robot.* **2013**, *29*, 625–640. [[CrossRef](#)]
63. Bialy, B.; Chakraborty, I.; Cekic, S.; Dixon, W. Adaptive boundary control of store induced oscillations in a flexible aircraft wing. *Automatica* **2016**, *70*, 230–238. [[CrossRef](#)]
64. Siranosian, A.; Krstic, M.; Smyshlyaev, A.; Bement, M. Motion planning and tracking for tip displacement and deflection angle for flexible beams. *J. Dyn. Syst. Meas. Control ASME* **2009**, *131*, 1–10. [[CrossRef](#)]
65. Gao, S.; Liu, J. Adaptive neural network vibration control of a flexible aircraft wing system with input signal quantization. *Aerosp. Sci. Technol.* **2020**, *96*, 105593. [[CrossRef](#)]
66. Bu, X.; Qi, Q. Fuzzy Optimal Tracking Control of Hypersonic Flight Vehicles via Single-Network Adaptive Critic Design. *IEEE Trans. Fuzzy Syst.* **2022**, *30*, 270–278. [[CrossRef](#)]
67. Bu, X.; Xiao, Y.; Lei, H. An Adaptive Critic Design-Based Fuzzy Neural Controller for Hypersonic Vehicles: Predefined Behavioral Nonaffine Control. *IEEE/ASME Trans. Mechatronics* **2019**, *24*, 1871–1881. [[CrossRef](#)]

**Disclaimer/Publisher’s Note:** The statements, opinions and data contained in all publications are solely those of the individual author(s) and contributor(s) and not of MDPI and/or the editor(s). MDPI and/or the editor(s) disclaim responsibility for any injury to people or property resulting from any ideas, methods, instructions or products referred to in the content.